



This is a repository copy of *Kinetic studies of the methanation of CO over a Ni/γ-Al₂O₃ catalyst using a batch reactor.*

White Rose Research Online URL for this paper:
<http://eprints.whiterose.ac.uk/95053/>

Version: Accepted Version

Article:

Lim, J.Y, McGregor, J., Sederman, J. et al. (1 more author) (2016) Kinetic studies of the methanation of CO over a Ni/γ-Al₂O₃ catalyst using a batch reactor. Chemical Engineering Science. ISSN 0009-2509

<https://doi.org/10.1016/j.ces.2016.02.001>

Article available under the terms of the CC-BY-NC-ND licence
(<https://creativecommons.org/licenses/by-nc-nd/4.0/>)

Reuse

Unless indicated otherwise, fulltext items are protected by copyright with all rights reserved. The copyright exception in section 29 of the Copyright, Designs and Patents Act 1988 allows the making of a single copy solely for the purpose of non-commercial research or private study within the limits of fair dealing. The publisher or other rights-holder may allow further reproduction and re-use of this version - refer to the White Rose Research Online record for this item. Where records identify the publisher as the copyright holder, users can verify any specific terms of use on the publisher's website.

Takedown

If you consider content in White Rose Research Online to be in breach of UK law, please notify us by emailing eprints@whiterose.ac.uk including the URL of the record and the reason for the withdrawal request.

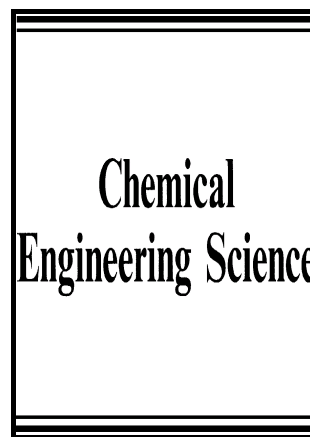


eprints@whiterose.ac.uk
<https://eprints.whiterose.ac.uk/>

Author's Accepted Manuscript

Kinetic studies of the methanation of CO over a Ni/ γ -Al₂O₃ catalyst using a batch reactor

Jin Yang Lim, J. McGregor, A.J. Sederman, J.S. Dennis



www.elsevier.com/locate/ces

PII: S0009-2509(16)30046-X
DOI: <http://dx.doi.org/10.1016/j.ces.2016.02.001>
Reference: CES12793

To appear in: *Chemical Engineering Science*

Received date: 28 October 2015

Revised date: 10 January 2016

Accepted date: 2 February 2016

Cite this article as: Jin Yang Lim, J. McGregor, A.J. Sederman and J.S. Dennis
Kinetic studies of the methanation of CO over a Ni/ γ -Al₂O₃ catalyst using
batch reactor, *Chemical Engineering Science*
<http://dx.doi.org/10.1016/j.ces.2016.02.001>

This is a PDF file of an unedited manuscript that has been accepted for publication. As a service to our customers we are providing this early version of the manuscript. The manuscript will undergo copyediting, typesetting, and review of the resulting galley proof before it is published in its final citable form. Please note that during the production process errors may be discovered which could affect the content, and all legal disclaimers that apply to the journal pertain.

Kinetic studies of the methanation of CO over a Ni/ γ - Al_2O_3 catalyst using a batch reactor

Jin Yang Lim¹, J. McGregor², A. J. Sederman¹, J. S. Dennis¹

¹ Department of Chemical Engineering and Biotechnology, University of Cambridge, Cambridge CB2 3RA, United Kingdom.

² Department of Chemical and Biological Engineering, The University of Sheffield, Sir Robert Hadfield Building, Portobello Street, Sheffield, S1 3JD, United Kingdom.

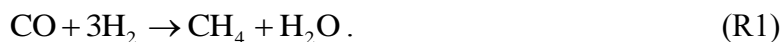
Abstract

The methanation of CO was investigated in a gradientless, spinning-basket reactor at temperatures 443 – 473 K and pressures up to 16 bar. The reactor was operated in batch and the composition of its contents was determined periodically. Temperature programmed studies and DRIFTS analysis were performed to gain an understanding of the nature of the surface of the catalyst. In all experiments, the reaction initially proceeded with a constant rate period. This was followed by a marked increase in the rate of production of CH_4 after the depletion of CO, attributed to the hydrogenation of remaining carbonyl groups on the surface as well as the hydrogenolysis of long-chained paraffins in the reactor. The selectivity for CH_4 was found to be significantly lower than that observed in CO_2 methanation, consistent with the low H_2 to CO ratio on the surface of the catalyst. Temperature-programmed studies and DRIFTS studies of the spent catalyst identified two main types of carbonaceous species on the surface of the catalyst, with the results being consistent with the presence of (i) carbonyl species on nickel clusters and (ii) formate groups on nickel sites which have a stronger interaction with the alumina support. The former were found to be reactive at the temperatures studied. Finally, the rate of methanation was found to be insensitive to H_2O . This was attributed to the strong affinity of the nickel catalyst for CO, which saturates the surface of the catalyst leaving little opportunity for the adsorption of H_2O . Two models were derived assuming that the rate-limiting steps was either (i) the adsorption of H_2 on the catalyst, or (ii) the reaction of gaseous H_2 with adsorbed CO. The strong adsorption of CO on the surface of the catalyst, evident from various experimental observations, is consistent with both mechanisms.

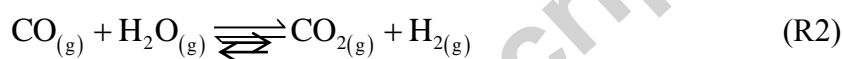
Keywords: methanation of CO; batch reactor experiments; Ni/ γ alumina catalyst; reaction kinetics; modelling

1. Introduction

The methanation of CO, viz. the production of CH₄ from the reaction between CO and H₂, is important in satisfying the increasing demand for synthetic natural gas (SNG):



A number of transition metals have been shown to be active in catalysing Reaction (1), including Ni, Ru, Rh, Pt and Co (Vannice, 1975; Khodakov et al., 2007; Tada and Kikucha, 2015). Nickel-based catalysts remain promising candidates for methanation reactions in industrial processes because of their high activity and low cost. The reaction of CO and H₂ over a nickel-based catalyst is less selective towards methane than is CO₂ methanation (Weatherbee and Barholomew, 1981). Side reactions include the water-gas shift reaction (R2), the Boudouard reaction (R3) and polymerisation to higher hydrocarbons (R4):



Two main mechanisms, illustrated in Figure 1, have been proposed in the literature for the methanation of CO:

- (i) The first involves adsorbed CO dissociating to adsorbed carbon and oxygen, which are hydrogenated to CH₄ and H₂O (e.g. Ho and Harriet, 1980; Klose and Baerns, 1984; Sughrue and Barholomew, 1982, Tada and Kikucha, 2015).
- (ii) The second mechanism involves an oxygenated species, such as a COH_x complex. Figure 1 (ii) shows an example of the reaction scheme proposed by Vannice (1975), where an enol intermediate was proposed.

Araki and Ponc (1976) studied the rate of hydrogenation of surface carbon species by admitting a known volume of ¹³CO to a clean Ni film followed by the introduction of a reaction mixture of H₂ and ¹²CO₂. They found that ¹³CH₄ was produced immediately after the mixture of H₂ and ¹²CO₂ was introduced whilst ¹²CH₄ was produced only after an induction period. The increase in the amount of ¹²CH₄ produced was accompanied by the formation of ¹²CO₂; however, no ¹³CO₂ was detected. This suggests that adsorbed carbon does not recombine with oxygen to form CO or CO₂ molecules. Also, CO dissociates into surface

carbon and oxygen from the observations that the Boudouard reaction is active on nickel catalysts above 250°C (Tøttrup, 1976; Rostrup-Nielsen and Trimm, 1977; Gardner and Bartholomew, 1981). While many agree that mechanism (i) is a reasonable description, different kinetic rate expressions have been proposed based on different assumptions of the rate-limiting steps and the species present (Ho and Harriet, 1980; Klose and Baerns, 1984; Sughrue and Bartholomew, 1982; Xu and Froment, 1989), discussed later in this paper.

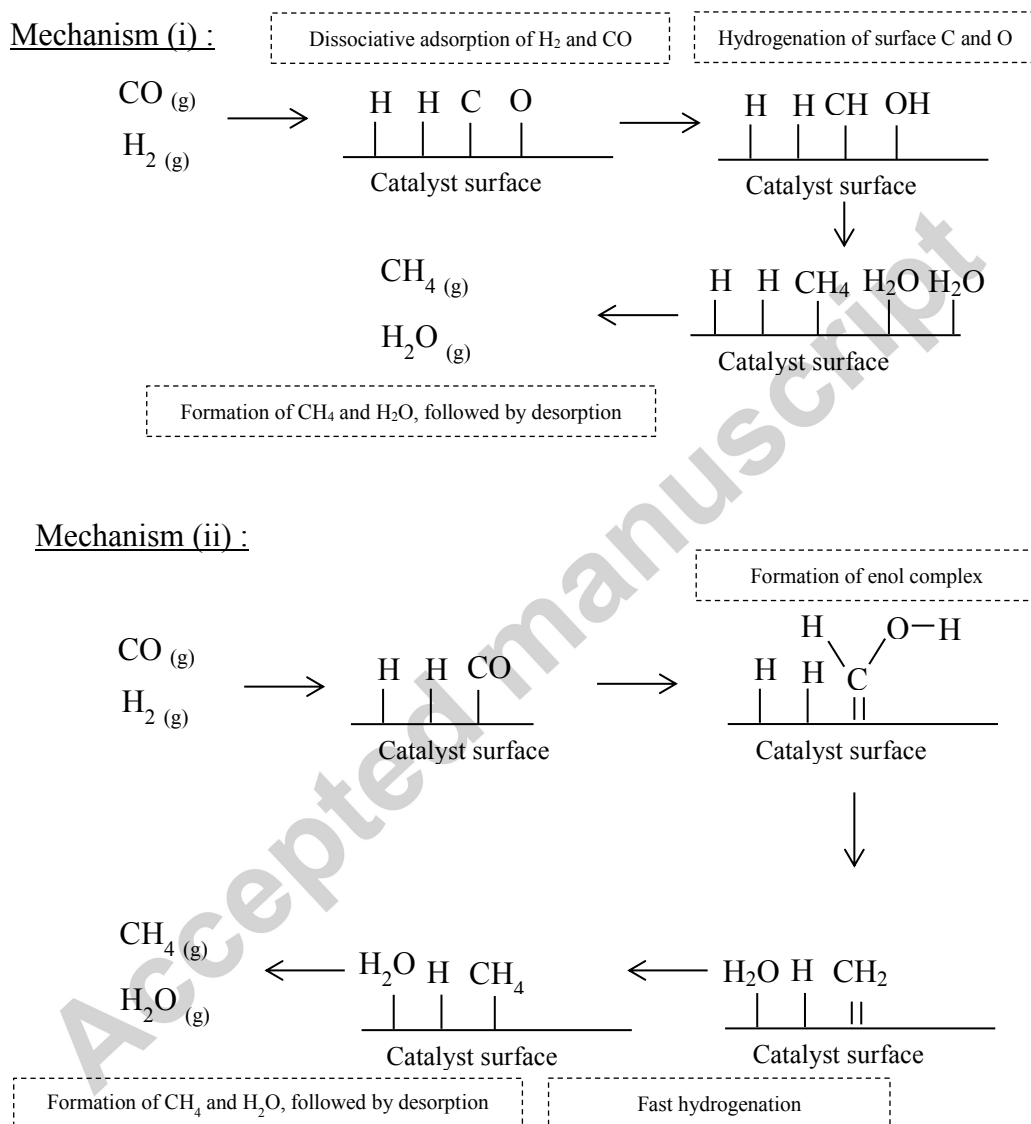


Figure 1. Schematic diagram of reaction mechanisms for CO methanation (i) via the dissociative adsorption of CO, (ii) via an enol intermediate.

Vannice (1975), van Herwijnen et al. (1973) and Huang and Richardson (1977) proposed rate expressions consistent with mechanism (ii). Further evidence for the presence of an oxygenated intermediate can be found in infra-red (IR) studies. Sanchez-Escribano et al. (2007) studied the nature of the surface species present on a supported 10 wt% Ni/Al₂O₃

catalyst, under operando conditions in an IR cell. A mixture of CO and H₂ was passed over the catalyst bed and the FT-IR spectra of the adsorbed species were obtained at different reaction temperatures. Significant IR bands for formate and carbonate groups were observed, indicating the presence of oxygenated species on the surface. They also found that methane was produced after a catalyst sample pre-treated with methanol was heated in H₂, suggesting that oxygenated species formed from the adsorption of methanol follow a certain reaction to form CH₄. Similar IR bands were observed by Fujita et al. (1993), who noted that the amounts of linear carbonyl species were much larger in CO methanation compared to CO₂ methanation and suggested that the presence of a considerable amount of carbonyl species on the surface inhibits the rate of CO methanation. Using density functional theory calculations (DFT) on different model surfaces of nickel, Andersson et al. (2008) showed that the dissociation of CO via a COH complex has a slightly lower activation energy compared with the direct dissociation of CO to adsorbed C and O. They also showed that at temperatures higher than 850 K, the rate-limiting step became the hydrogenation of surface carbon, consistent with the observations by Sughrue and Barholomew (1982).

Further investigation is necessary to improve understanding of CO methanation. The aim of this paper was to obtain a representative kinetic expression valid over a wide range of partial pressures of CO and H₂. A way of validating rate expressions is to examine their applicability over a wide range of partial pressures of reactants and products, conveniently achieved by conducting the reaction in a batch reactor (Lim et al. 2015). Here, we have studied the kinetics of the methanation of CO₂ in a gradientless, spinning-basket reactor operating in batch.

2. Experimental

2.1 Materials, apparatus and method

The catalyst, reduced 12 wt% Ni/ γ -Al₂O₃, was synthesised as described in detail by Lim et al. (2015), who also give details of the apparatus and technique employed. Information on the characterisation of the catalyst is given in Supplementary Information Section 1. The total available surface area and the pore size distribution was measured by gas adsorption analysis and determined using the BET and BJH models. Temperature programmed studies were performed by off-gas analysis in a CATLAB microreactor and in a thermogravimetric analyser (TGA) in order to determine the different oxidation states within the samples. The TGA was also used to confirm the mass fraction of Ni in the fully oxidised sample and

determine the fraction of metallic Ni which could be oxidised at room temperature. Powder X-ray diffraction (XRD) was used to determine the different crystalline phases within the solid samples. The dispersion of surface Ni on the sample was measured by pulse H₂ chemisorption experiments, which was performed in the CATLAB apparatus.

Reaction studies were undertaken in a Carberry, spinning basket reactor to study the behaviour of the catalyst in the presence of CO, H₂O or both. Depending on the experiments, gas from cylinders containing (i) 24 vol% CO, 4 vol% Ar, H₂ balance (± 2 vol% precision, BOC), (ii) pure H₂ (99.99 vol% purity, Air Liquide), (iii) CO₂ (99.99 vol% purity, Air Liquide), (iv) CO (BOC), (v) CH₄ (99.5 vol% purity, Air Liquid), (vi) N₂ (99.998 vol% purity, Air Liquide) and (v) Ar (99.998 vol% purity, Air Liquide) was used to pressurise the reactor.

In a typical experiment, the basket in the reactor was first loaded with a known amount of catalyst and packed with a non-porous, inert glass beads (1.4 mm diam.), such that about 5.0 g of catalyst pellets were mixed with an equal mass of glass beads in the basket. The reactor was sealed, evacuated using a vacuum pump and then heated to 250°C. The catalyst was then subjected to a flow through the reactor of 100 ml/min (at room temperature and pressure) of H₂ with stirring at 1.7 Hz for 12 hours at 1 bar. Following reduction in H₂, the reactor was evacuated again and the internal temperature of the reactor brought to the desired reaction temperature. The rate of the reaction of interest was studied in batch by bringing the reactor to a desired initial pressure and composition, using gas supplied from cylinders connected to the reactor. A protocol for introducing gas was developed, described by Lim et al. (2015), which resulted in the final pressure of the reactor being consistently achieved with a precision of ± 0.1 bar. A stirrer speed of 9.2 Hz was always used. The entire process of bringing the reactor to the desired pressure and starting the stirrer after the introduction of the gases typically took 10 – 15 s.

After the reactive gases were introduced into the reactor, the changes in the composition of its contents were measured over time. This was performed by taking volumes of 4 ± 0.2 ml (at atmospheric temperature and pressure) from the sampling line leading from the reactor using a gas-tight sampling syringe. Prior to the removal of the sample by the syringe, the gaseous contents of the sampling lines were evacuated by the vacuum pump. Gas from the reactor was then allowed into the sampling line. The gas collected was evacuated once again before the actual sample was taken. This procedure ensured that the composition of the sample of gas obtained from the reactor was representative of the contents of the bulk phase

of the reactor volume. Only about 6 – 10 samples were taken for each experiment in order to minimise the errors incurred from the removal of gaseous contents from the reactor. The composition of the sample was analysed using off-line gas chromatography (Agilent 7890 GC Extended Refinery Gas Analysis) by passing the sample in the syringe through the sampling loop in the gas-chromatograph. The sampling loop in the gas chromatograph was evacuated using a vacuum pump before the gaseous contents of the syringe were introduced.

The composition of the gas given by off-line gas chromatography is only equal to the bulk phase of the reactor if all species in the gas phase are above their dew point at room temperature and pressure. This was not the case for most reactions performed because water was involved as a product or a reactant. Since the analysis by gas chromatography provided a water-free composition of the gas, the partial pressures of different species in the gas phase of the reactor were determined by using argon as an internal standard, such that

$$p_i = \frac{x_i}{x_{Ar}} \times p_{Ar,0} \quad (1)$$

where p_i is the partial pressure of species i , x_i is the mole fraction of species i in the syringe, x_{Ar} is the mole fraction of Ar in the syringe and $p_{Ar,0}$ is the partial pressure of argon at the start of the reaction. In most experiments, gas cylinders (of different mixtures of H₂, CO₂ and CO) contained 4% Ar. Hence, $p_{Ar,0}$ could be easily determined by measuring the total pressure of the reactor and multiplying with the known composition of the cylinder.

2.2 Parameters affecting the measurement of kinetics

2.2.1 Control experiments

The collective catalytic activity of the supporting Al₂O₃, the interior surface of the reactor and the nickel oxides present in the catalyst was investigated for the methanation of CO. Thus, 5.0 g of the support (3 mm dia. SA-62125 alumina spheres, Saint-Gobain) was mixed with 5.0 g of non-porous glass beads (1.4 mm diam.). The Carberry reactor was evacuated and then 7.2 bar of H₂, 2.4 bar CO and 0.4 bar Ar was admitted to the evacuated reactor. The composition of the reactor was measured periodically by taking small samples of the gas from the reactor volume analysed by offline gas chromatography as described above. At both 293 and 463 K, no significant decreases in p_{CO} and p_{H_2} were observed, indicating that no reaction of CO and H₂ had occurred. Tiny increases in the partial pressure of methane were observed when the experiment was performed at 463 K with only the support, i.e. the alumina

spheres and when the experiment was performed with the fully-oxidised catalyst Ni/Al₂O₃. However, the maximum amount of methane observed was 1.5×10^{-4} bar after 6361 s, significantly smaller than that observed when a similar mass of active catalyst was used. It was therefore concluded that the oxidised form of the catalyst was inactive in the catalysis of CO methanation and that the support material used in the synthesis of the Ni/Al₂O₃ catalyst, the interior surface of the reactor and the nickel oxides present in the catalyst could collectively be taken as inert compared to the reduced nickel catalyst.

2.2.1 Catalyst deactivation

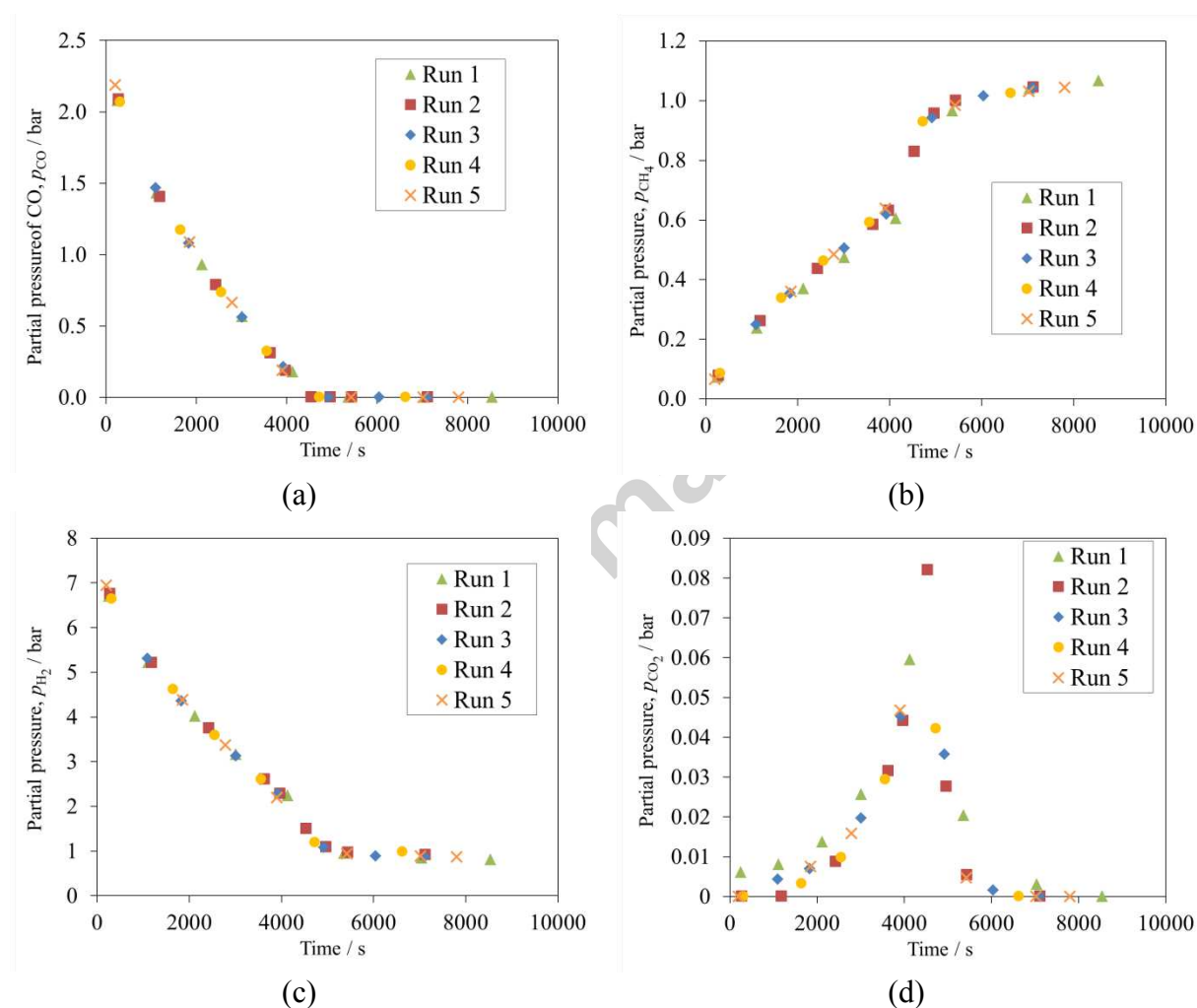


Figure 2. Partial pressure of (a) CO, (b) CH₄, (c) H₂ and (d) CO₂ with time for 5 consecutive runs in batch for the same catalyst: $p_{CO,0} = 2.4$ bar, $p_{H_2,0} = 7.2$ bar, $T = 463$ K, 5 g catalyst

Replicate experiments were performed using the same batch of catalyst for five repeated runs. Figure 2 shows the variation of the partial pressures of CO, H₂, CH₄ and CO₂ as a function of time for five consecutive, replicate experiments at 463 K with $p_{CO,0}$, the initial partial pressure of CO, of 2.4 bar and $p_{H_2,0}$, the initial partial pressure of H₂, 7.2 bar. The profiles of

the partial pressures of CO, H₂, CH₄ and CO₂ for different runs are almost identical, illustrating that there was negligible deactivation for at least five experiments, corresponding to a total time on stream of 4×10^4 s. The insignificant rate of deactivation and good reproducibility of the replicate experiments meant that CO methanation experiments could be performed on the same batch of Ni/Al₂O₃ catalyst. It also shows that loss of nickel by the formation of nickel carbonyl, or by the migration of Ni by this compound, was not significant. However, the same batch of catalyst was used for no more than 10 experiments before being replaced by a fresh batch. CO₂ methanation, with an initial condition of $p_{\text{CO}_2,0} = 2.4$ bar and $p_{\text{H}_2,0} = 7.2$ bar at 463 K, was performed as a control for the final experiment on a given batch of catalyst. CO₂ methanation was used as the reference condition because the experiments were of shorter duration than those using CO. Also, Ni-based catalysts undergo less deactivation during the methanation of CO₂ methanation compared to that of CO (Chang et al., 1997; Zhang et al., 2013).

2.2.2 Effect of heat and mass transfer external to the catalyst particle

The effect of heat and mass transfer from the bulk gaseous phase of the reactor to the external surface of the catalyst pellet was studied by performing CO methanation reactions, with an initial condition of $p_{\text{CO}} = 2.4$ bar and $p_{\text{H}_2} = 7.2$ bar at 463 K, at different impeller speeds. At the extremes, the initial rate of production of CH₄ when the impeller was stationary was about 14% faster than at 9.3 Hz. There was very little difference in the behaviour of the reaction for spinning speeds higher than 7.1 Hz.

The methanation of CO is exothermic with $\Delta H_{298\text{K}}^\circ = -206$ kJ mol⁻¹ so that the decrease in the observed rate of reaction could have been attributable to the enhanced dissipation of heat with increased impeller speeds. To investigate whether heat transfer is significant during typical experimental conditions, the difference between the bulk temperature and the surface of the particle, ΔT_p , was estimated by a pseudo-steady heat balance on the catalyst pellet:

$$r' \Delta H_{T_\infty}^\circ \rho_{\text{cat}} \left(\frac{4\pi R_p^3}{3} \right) = h (4\pi R_p^2) \Delta T_p, \quad (2)$$

where r' is the specific rate of reaction, $\Delta H_{T_\infty}^\circ$ is the heat of reaction, T_∞ is the temperature of the bulk phase, ρ_{cat} is the density of the catalyst, R_0 is the radius of the pellet and h is the heat transfer coefficient. The initial rate of consumption of CO at the reference initial condition

$p_{\text{CO},0} = 2.4 \text{ bar}$, $p_{\text{H}_2,0} = 2.4 \text{ bar}$ and $T = 463 \text{ K}$ was determined experimentally to be $9.9 \times 10^{-4} \text{ mol kg}^{-1} \text{ s}^{-1}$. Values of the transport properties for the gas were based on a mixture of 75 vol% H_2 and 25 vol% CO at 463 K at 10 bar. For an isolated, spherical catalyst, diameter 3 mm, and an assumed superficial velocity of 0.9 m s^{-1} , $\text{Nu} = 30$ and the heat transfer coefficient was $\sim 1080 \text{ W m}^{-2} \text{ K}^{-1}$. Using Eq. (2), $\Delta T_p \sim 0.4 \text{ K}$. However, for a stationary particle, ΔT_p was $\sim 1.3 \text{ K}$, suggesting a very slight effect from heating effects. However, the empirical evidence showed there to be negligible differences in the response of the reaction in the batch reactor for impeller speeds $>7.1 \text{ Hz}$, so all experiments were performed using an impeller speed of 9.5 Hz . Thus, it could be assumed that there were negligible effects of heat and mass transfer from the bulk volume of the reactor to the surface of the catalyst.

2.2.3 Effect of intra-particle heat and mass transfer

Using a rate of consumption of CO during methanation at 463 K of $9.9 \times 10^{-4} \text{ mol kg}^{-1} \text{ s}^{-1}$ and an average pore diameter of 8.9 nm, the Weisz-Prater number (Weisz and Prater, 1954)

$$N_{\text{WP}} = \frac{r' \rho_{\text{cat}} R_p^2}{C_s D_{\text{eff}}}, \quad (3)$$

was ~ 0.008 , much smaller than the estimated threshold of 0.3 at which mass transfer limitations are expected to become significant. Here, C_s was the concentration of CO in mol m^{-3} . Given the small pore diameter, the effective diffusivity, D_{eff} , was taken to be the product of the Knudsen diffusivity of CO and (ε/τ^2) , with $\varepsilon = 0.60$ and τ^2 assumed to be 3. Here, ε was determined from the cumulative pore volume of the Al_2O_3 support, accounting for pores ranging from 17 to 300 nm in diameter, of $0.55 \text{ cm}^3 \text{ g}^{-1}$. The group (ε/τ^2) is appropriate for use with the model of Young and Todd (2005) to model diffusion within the particle of catalyst.

To estimate the temperature difference between the centre and the surface of the pellet, the model of reaction and diffusion in a catalyst pellet of Lim and Dennis (2012) was solved for the extreme case of constant kinetics of $9.9 \times 10^{-4} \text{ mol}_{\text{CO}} \text{ kg}^{-1} \text{ s}^{-1}$, with conditions at the surface of the pellet taken to be $p_{\text{CO}} = 2.4 \text{ bar}$ and $p_{\text{H}_2} = 7.2 \text{ bar}$. The effective thermal conductivity of the pellet was taken as the thermal conductivity of Al_2O_3 , $9 \text{ W m}^{-1} \text{ K}^{-1}$. At 463 K, the estimated temperature difference between the centre and the surface of the catalyst pellet was only about 0.1 K for a pellet with a diameter of 3 mm, indicating that intraparticle temperature gradients are negligible. This conclusion was substantiated experimentally by measuring the change in partial pressure of H_2 and CH_4 as a function of time for two different

particle sizes at the reference initial condition of $p_{\text{CO}_2,0} = 2.4$ bar and $p_{\text{H}_2,0} = 7.2$ bar at 463 K. The behaviour of the 3 mm dia. pellet was equal to that of the 1.7 – 2.3 mm pellets, suggesting that intra-particle mass transfer limitations were small.

2.2.4 Effect of total pressure

The effect of total pressure was investigated by comparing the experimental results methanation for different initial partial pressures of the inert gas N_2 , first admitted to the evacuated vessel before the CO and H_2 were introduced at 463 K. There was no observable effect of total pressure on the CO methanation reaction for partial pressures of N_2 up to 6 bar.

3 Results

3.1 General features

This section reports the transient profiles of the partial pressures of various gaseous species in the batch reactor at the reference initial condition, i.e. $p_{\text{CO},0} = 2.4$ bar, $p_{\text{H}_2,0} = 7.2$ bar at $T = 463$ K, which has been illustrated in Figure 2. Figures 2(a) and (c) show that for $t < 4000$ s, the decreases in p_{CO} and p_{H_2} were approximately linear with time. The corresponding increase in p_{CH_4} was also found to be largely linear, as seen in Figure 2 (b). At $t \approx 4500$ s, p_{CO} was depleted. After this time, a marked increase in the rate of formation of methane, accompanied by a decrease in the rate of reaction of H_2 , was observed. The variation of p_{CO_2} with time, Figure 2 (d), featured an initial rapid increase in p_{CO_2} with time for $t < 4000$ s. However, an extremely sharp decrease in p_{CO_2} was observed at approximately 4500 s, coinciding with the depletion of CO in the gas phase.

The origin of the CO_2 is attributable to the water-gas shift reaction. Other results, Lim et al. (2016), indicated that the rate of the water-gas shift reaction, in an atmosphere with high p_{CO} , was found to increase with $p_{\text{H}_2\text{O}}$ and, with the exception of very low p_{CO} , viz. < 0.1 bar, p_{CO} had no effect on the on the rate. Figure 2 (d) shows that for an initial condition of $p_{\text{CO},0} = 2.4$ bar and $p_{\text{H}_2,0} = 7.2$ bar, the rate of production of CO_2 increased with time. This is the result of the production from the CO methanation of H_2O , which accumulates because of the batch operation. As $p_{\text{H}_2\text{O}}$ increased with time, the rate of formation of CO_2 increased correspondingly. This provides evidence that the water-gas shift reaction was responsible for

the formation of CO₂ in the reactor and not the Boudouard reaction, where experiments (Lim et al., 2016) gave a rate of production of CO₂ decreasing over time, contrary to Figure 2(d).

The carbon balance for the batch reaction is illustrated in Figure 3 (a). Here, the total amount of carbon in the gas phase in equivalent partial pressure, p_C , was calculated as

$$p_C = p_{CO} + p_{CO_2} + \sum_{i=1}^6 N_i p_{HC,i} \quad (4)$$

where $p_{HC,i}$ is the partial pressure of hydrocarbon i , and N_i is the carbon number of hydrocarbon i . It should be noted that the summation includes all paraffins and olefins detected by the gas chromatograph. The variation of p_C with time, plotted in Figure 3, represents the carbon balance of the CO methanation reaction in the batch reactor. It is clear that as the reaction proceeded, p_C decreased almost linearly with time, suggesting the formation of carbon species which could not be detected in the gas phase. When $p_{CO} = 0$, at $t \approx 4500$ s, p_C was observed to recover from about 1.8 bar to 2.1 bar. The overall carbon balance at the end of each experiment was approximately 87% of the original inventory, i.e. 2.4 bar of CO. The increase of p_C is mainly caused the marked increase in p_{CH_4} after the depletion of p_{CO} , as seen in Figure 2 (b). This is further supported by Figures 4 (a) and (b), where no significant increase in the partial pressures of C₂H₆ and C₃H₈ were found after $t \approx 4500$ s. Since the carbon balance of the reaction could not be fully addressed by all the species in the gas phase, the selectivity of the CO methanation reaction is best expressed as a fractional conversion of CO to species i , F_i , such that

$$F_i = \frac{p_{HC,i}}{(p_{CO,0} - p_{CO} + p_{CO_2})} \quad (5)$$

where $p_{CO,0}$ is the initial partial pressure of CO. Of course, the values of F_i , $p_{HC,i}$, p_{CO} and p_{CO_2} varied with time as the reaction proceeded and the variation of the F_i for different hydrocarbons is illustrated in Figure 5 (a). In this paper, the term ‘selectivity’ refers to the qualitative description of the product distribution while ‘fractional conversion’ is a quantitative value as defined by Eq. (5). It is noted that before $t \approx 4500$ s, there was a small increase in the fractional conversion towards CH₄, F_{CH_4} , from 0.23 to 0.27. However, a large increase in F_{CH_4} was observed after $t \approx 4500$ s, as expected from the earlier observations. The

fractional conversions for other paraffins remained largely constant over the course of the experiment. Figure 5 (b) shows the fractional conversion of different paraffins at the end of each experiment for the five replicate experiments. The distribution of the products appeared to decrease markedly with the carbon number of the paraffin. It should be noted that only very small quantities of olefins were detected (not shown), with partial pressures several orders of magnitudes smaller than the paraffin with the same carbon number.

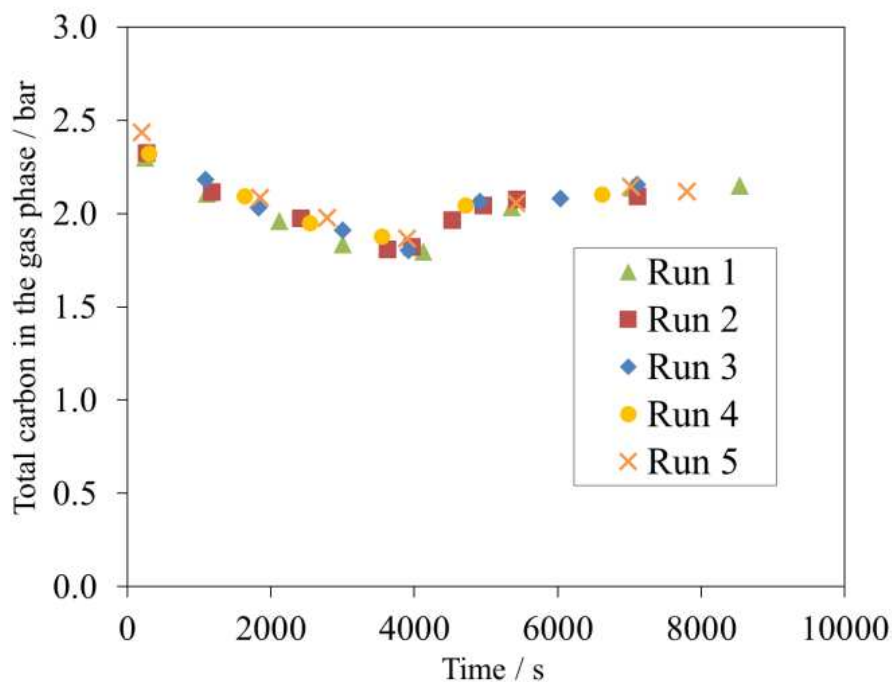


Figure 3. The variation of p_C with time for five replicate experiments. In all experiments, $p_{CO,0} = 2.4$ bar, $p_{H_2,0} = 7.2$ bar, $T = 463$ K and $m_{cat} = 5.0$ g.

The transition from the constant rate period before $p_{CO} = 0$ to the period after this time is a key feature in many of the experimental results illustrated in the following Sections. For convenience, the period before $p_{CO} = 0$ will be called period I and times thereafter period II.

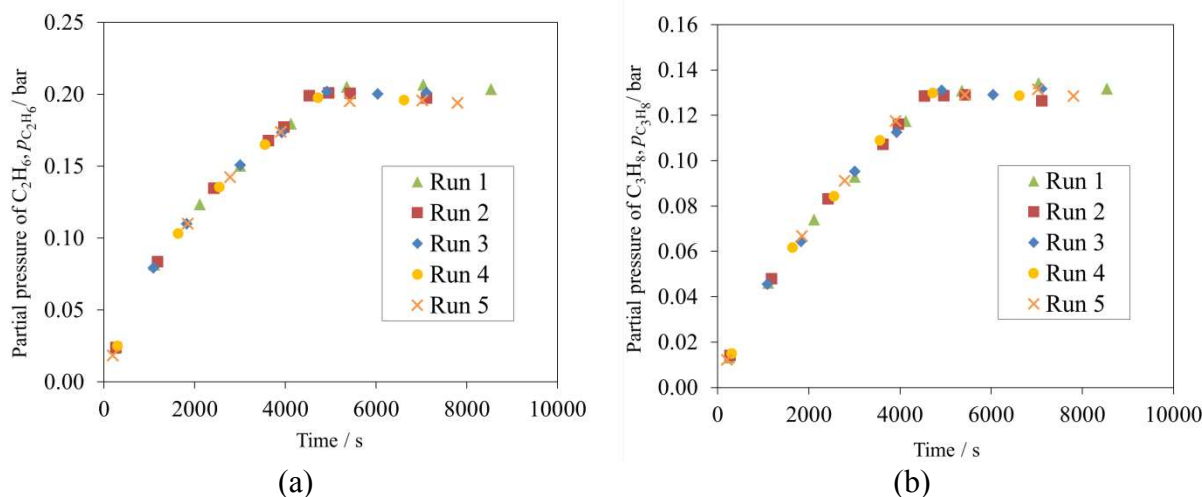


Figure 4. The partial pressure of (a) C_2H_6 and (b) C_3H_8 with time for 5 consecutive runs in batch for the same catalyst. In all experiments, $p_{CO,0} = 2.4$ bar, $p_{H_2,0} = 7.2$ bar, $T = 463$ K and $m_{cat} = 5.0$ g.

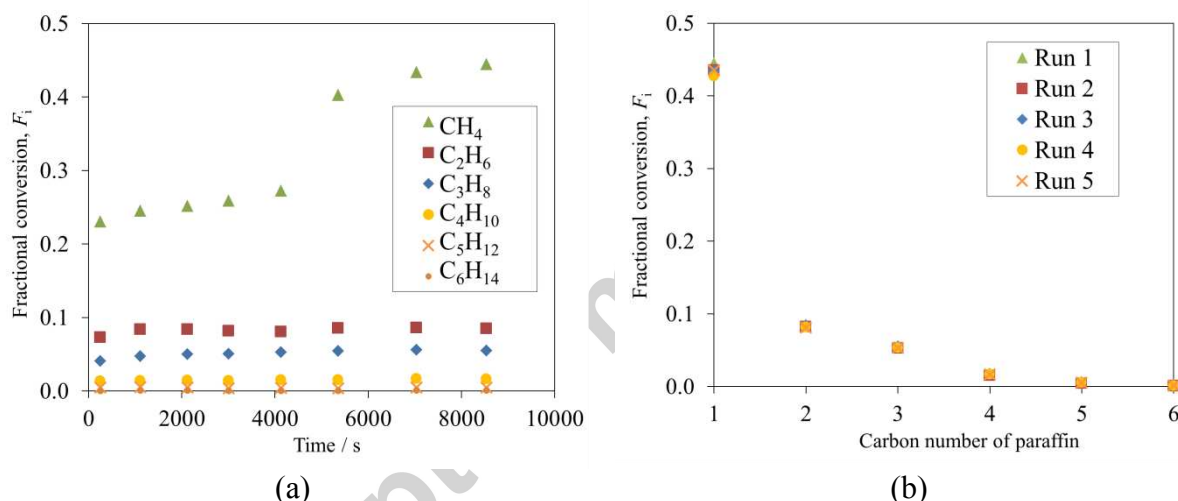


Figure 5. (a) The variation of the fractional conversion of different paraffins with time for Run 1. (b) The fraction conversion of paraffins of different carbon number at the end of each experiment. In all experiments, $p_{CO,0} = 2.4$ bar, $p_{H_2,0} = 7.2$ bar, $T = 463$ K and $m_{cat} = 5.0$ g.

3.2 Effect of p_{H_2}

The effect of p_{H_2} on the rate of CO methanation was studied by first raising the pressure of the evacuated reactor to a desired pressure with pure H_2 before a mixture of 24 vol% CO, 72 vol% H_2 and 4 vol% Ar was introduced. Figure 6 illustrates changes in the partial pressures of CO, H_2 , CH_4 and CO_2 over time for different initial partial pressures of H_2 . Figure 6 (a) shows that increasing the partial pressure of H_2 increased the rate of consumption of CO. In fact, the rate of consumption of CO increased from $9.4 \times 10^{-4} \text{ mol}_{CO} \text{ kg}^{-1} \text{ s}^{-1}$ with $p_{H_2,0} = 7.2$ bar to $1.34 \times 10^{-3} \text{ mol}_{CO} \text{ kg}^{-1} \text{ s}^{-1}$ when $p_{H_2,0} = 13.2$ bar, an increase of $\sim 30\%$.

Since the rate of consumption of CO was faster, the transition from period I to II also occurred earlier for higher partial pressures of H₂, reflected in the profiles of CO and CH₄ in Figure 6 (a) and (c). The maximum in p_{CO_2} with time also occurred earlier, consistent with the observation that the consumption of CO₂ occurred only when p_{CO} had fallen to zero.

The rate of production of CH₄ was significantly greater than the increase in the rate of consumption of CO with higher partial pressure of H₂. The initial rate of production of CH₄ when $p_{\text{H}_2,0} = 7.2$ bar was $2.3 \times 10^{-4} \text{ mol}_{\text{CH}_4} \text{ kg}^{-1} \text{ s}^{-1}$ increasing by a factor of 2.3 to $5.2 \times 10^{-4} \text{ mol}_{\text{CH}_4} \text{ kg}^{-1} \text{ s}^{-1}$ when $p_{\text{H}_2,0} = 13.2$ bar, significantly higher than the increase in the rate of consumption of CO as noted earlier. The marked increase in the rate of production of CH₄ is the result of (i) the inherent increase in the rate of reaction and (ii) the increase in the selectivity towards methane, both a result of the higher ratio of partial pressure of H₂ to CO.

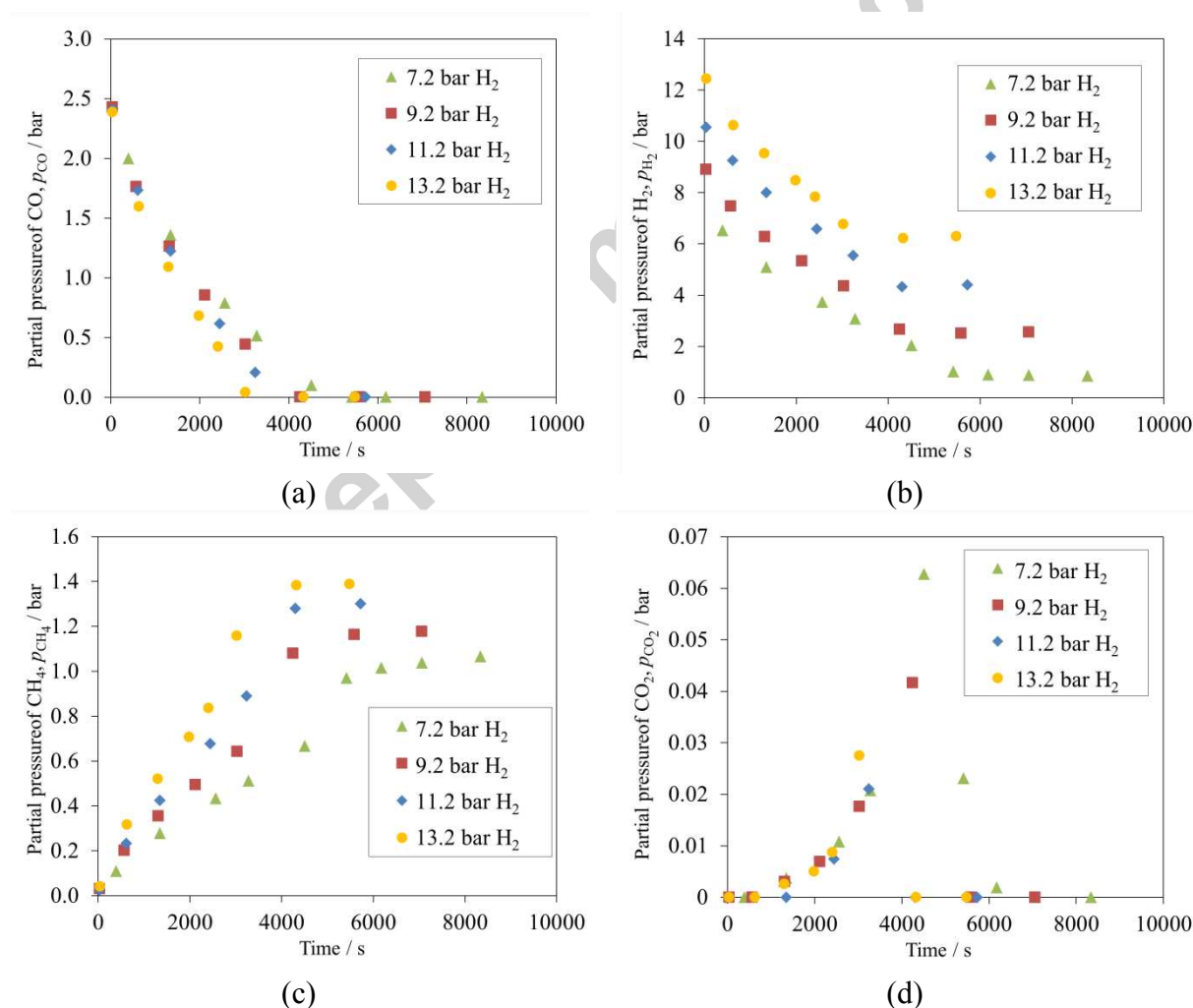


Figure 6. The variation of the partial pressure of (a) H₂, (b) CO, (c) CH₄ and (d) CO₂ over time for different initial partial pressures of H₂. $p_{\text{CO},0} = 2.4$ bar, $T = 463$ K and $m_{\text{cat}} = 5.0$ g.

The effect of increasing p_{H_2} on the selectivity towards CH_4 can be observed in Figure 7(a), where the fractional conversion increased significantly with $p_{\text{H}_2,0}$. The increase in selectivity towards CH_4 was prevalent throughout the length of the experiment, viz. for higher $p_{\text{H}_2,0}$, the fractional conversion for CH_4 was higher in both period I and II. Figures 7 (b), (c) and (d) illustrate the fractional conversions of ethane, propane and n-butane over time for different $p_{\text{H}_2,0}$. There was no significant change in the selectivity towards the higher hydrocarbons for the range of p_{H_2} explored, with only a small decrease in the selectivity of propane and n-butane for higher $p_{\text{H}_2,0}$. Unlike the case with CH_4 , the fractional conversions of higher hydrocarbons remained largely constant for the duration of the reaction and no significant changes were observed after the depletion of p_{CO} . The overall carbon balance, represented by p_{C} , appeared to be closer to the initial value of $p_{\text{C}} = 2.4$ bar with higher partial pressures of H_2 as illustrated in Figure 8 and consistent with the observation that more CH_4 was produced. This also suggests that with higher p_{H_2} , there was a smaller rate of formation of liquid hydrocarbons or surface carbonaceous species which led to more gaseous hydrocarbons.

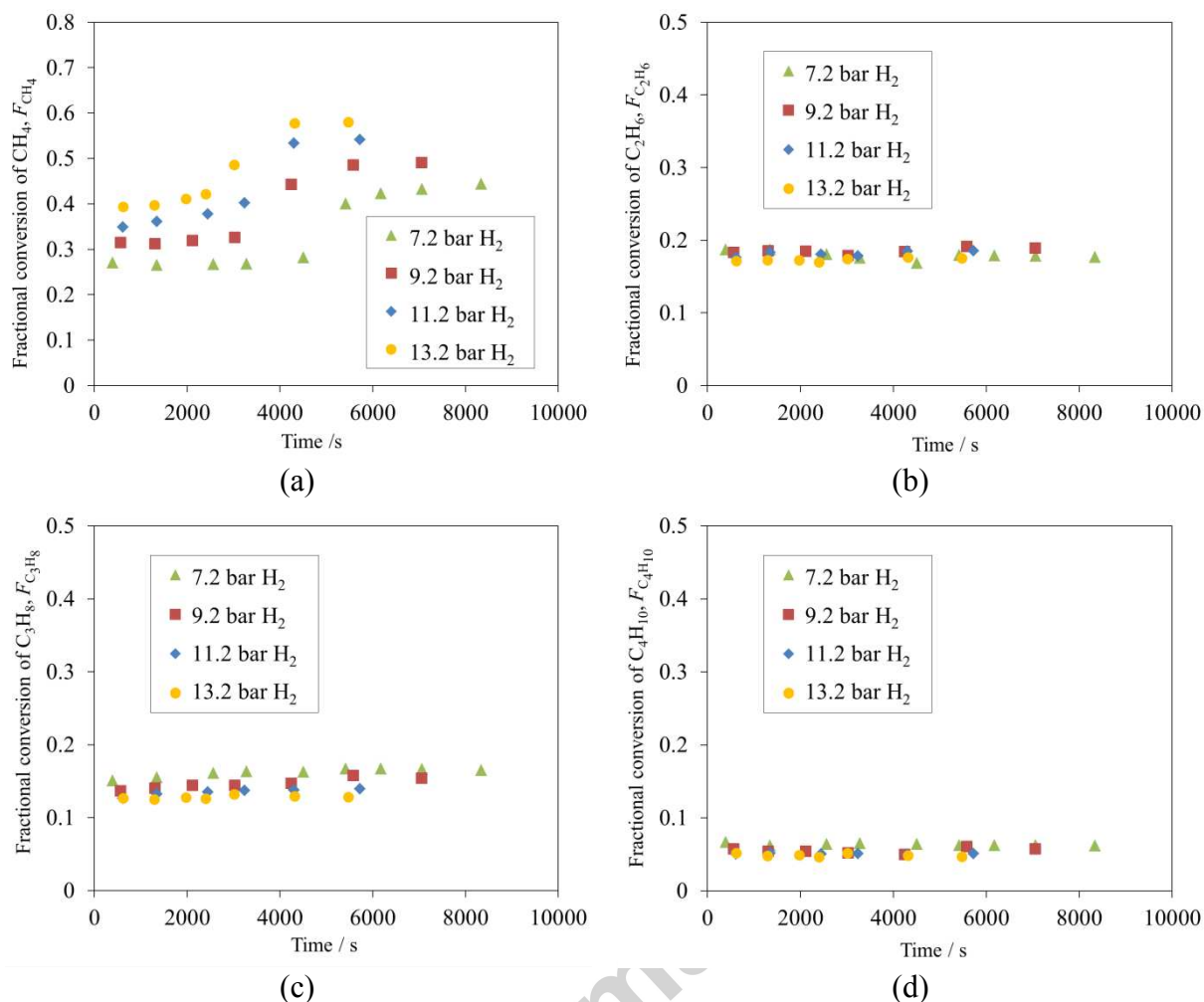


Figure 7. Fractional conversion of (a) CH₄, (b) C₂H₆, (c) C₃H₈ and d) C₄H₁₀ function of the conversion of CO, X_{CO} , for different initial partial pressures of H₂. $p_{H_2,0} = 7.2$ bar, $T = 463$ K and $m_{cat} = 5.0$ g.

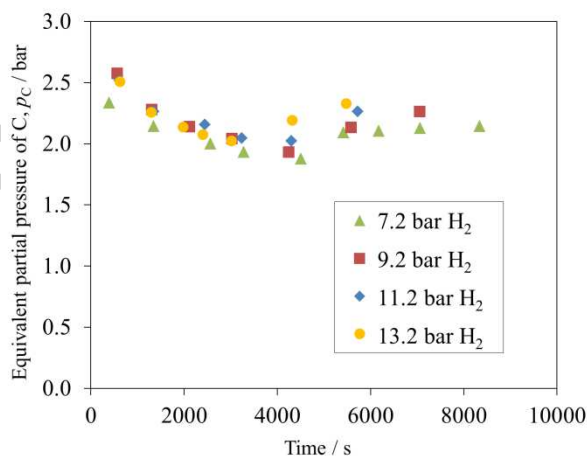


Figure 8. Variation of equivalent partial pressure of total carbon in the gas phase, p_C , versus time for different initial partial pressures of H₂. $p_{CO,0} = 2.4$ bar, $T = 463$ K and $m_{cat} = 5.0$ g.

3.3 Effect of p_{CO}

Here, the pressure of the reactor was raised to a desired pressure with pure CO before the introduction of the mixture of CO and H₂ in order to study the effects of variations in p_{CO} . Figure 9 shows that the rate of reaction, calculated from the rate of consumption of p_{H_2} or the rate of production of p_{CH_4} , decreased as the initial partial pressure of CO, $p_{\text{CO},0}$, increased. The initial rate of production of CH₄ decreased from $2.3 \times 10^{-4} \text{ mol}_{\text{CH}_4} \text{ kg}^{-1} \text{ s}^{-1}$ at $p_{\text{CO},0} = 2.4 \text{ bar}$ to $1.6 \times 10^{-4} \text{ mol}_{\text{CH}_4} \text{ kg}^{-1} \text{ s}^{-1}$ when $p_{\text{CO},0} = 5.8 \text{ bar}$. When $p_{\text{CO},0} \geq 4.0 \text{ bar}$, the stoichiometry of the reaction resulted in the limiting species changing from CO to H₂. No transitions from period I to II were observed in experiments when $p_{\text{CO},0} \geq 4.0 \text{ bar}$, because in those experiments p_{CO} was never depleted and remained in excess in the reactor after the depletion of p_{H_2} . No abrupt changes in the rate of increase of p_{CH_4} were observed in Figure 9 (c) when CO was in excess. It was also noted that, for $p_{\text{CO},0} \geq 4.0 \text{ bar}$, p_{CO_2} continued to increase for the duration of the reaction, consistent with the observation that the consumption of CO₂ only occurs after CO has been depleted.

Figure 10 illustrates the selectivity for CH₄, C₂H₆, C₃H₈ and C₄H₁₀ for different initial partial pressures of CO at 463 K. Figure 10 (a) shows that for $p_{\text{CO},0} = 4.0$ and 5.8 bar, the selectivity of CH₄ remained largely constant at about 0.22 ± 0.01 over the course of the reaction. This was significantly lower than the fractional conversion of CH₄ when $p_{\text{CO},0} = 2.4 \text{ bar}$. The selectivities for the higher hydrocarbons were also found to be smaller when $p_{\text{CO},0}$ was increased. However, in all cases, the product distribution of the reaction when $p_{\text{CO},0} = 4.0$ was identical to that when $p_{\text{CO},0} = 5.8 \text{ bar}$. As expected, the total amount of carbon in the gas phase, p_{C} , decreased monotonically over time for $p_{\text{CO},0} = 4.0$ and 5.8 bar (results given in Supplementary Information, Section 2), suggesting a build up of liquid hydrocarbons in the reactor or carbonaceous species on the catalyst. No recovery of p_{C} was observed when CO was in stoichiometric excess.

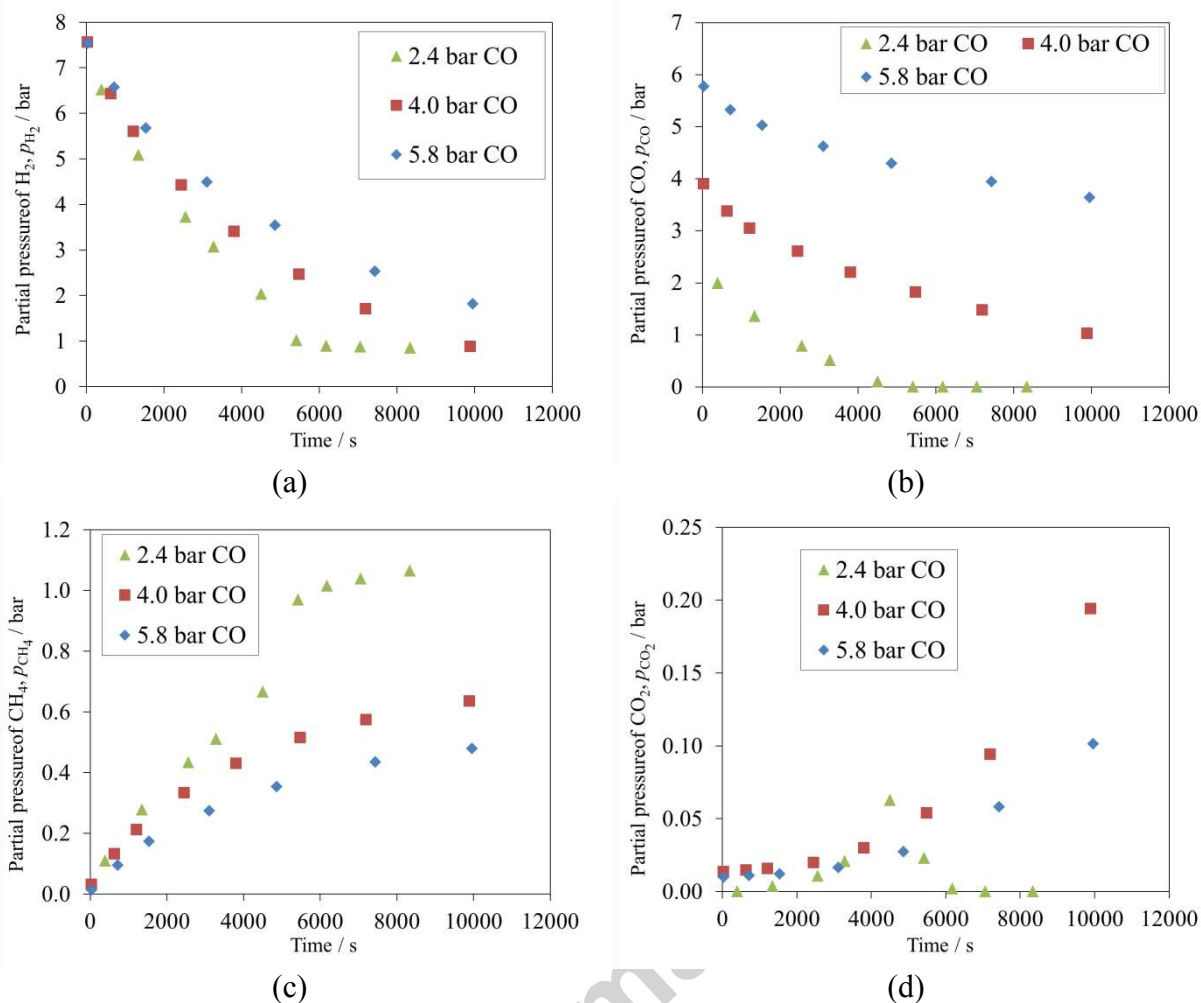


Figure 9. The variation of the partial pressure of (a) H₂, (b) CO, (c) CH₄ and (d) CO₂ over time for different initial partial pressures of CO. $p_{\text{H}_2,0} = 7.2$ bar, $T = 463$ K and $m_{\text{cat}} = 5.0$ g.

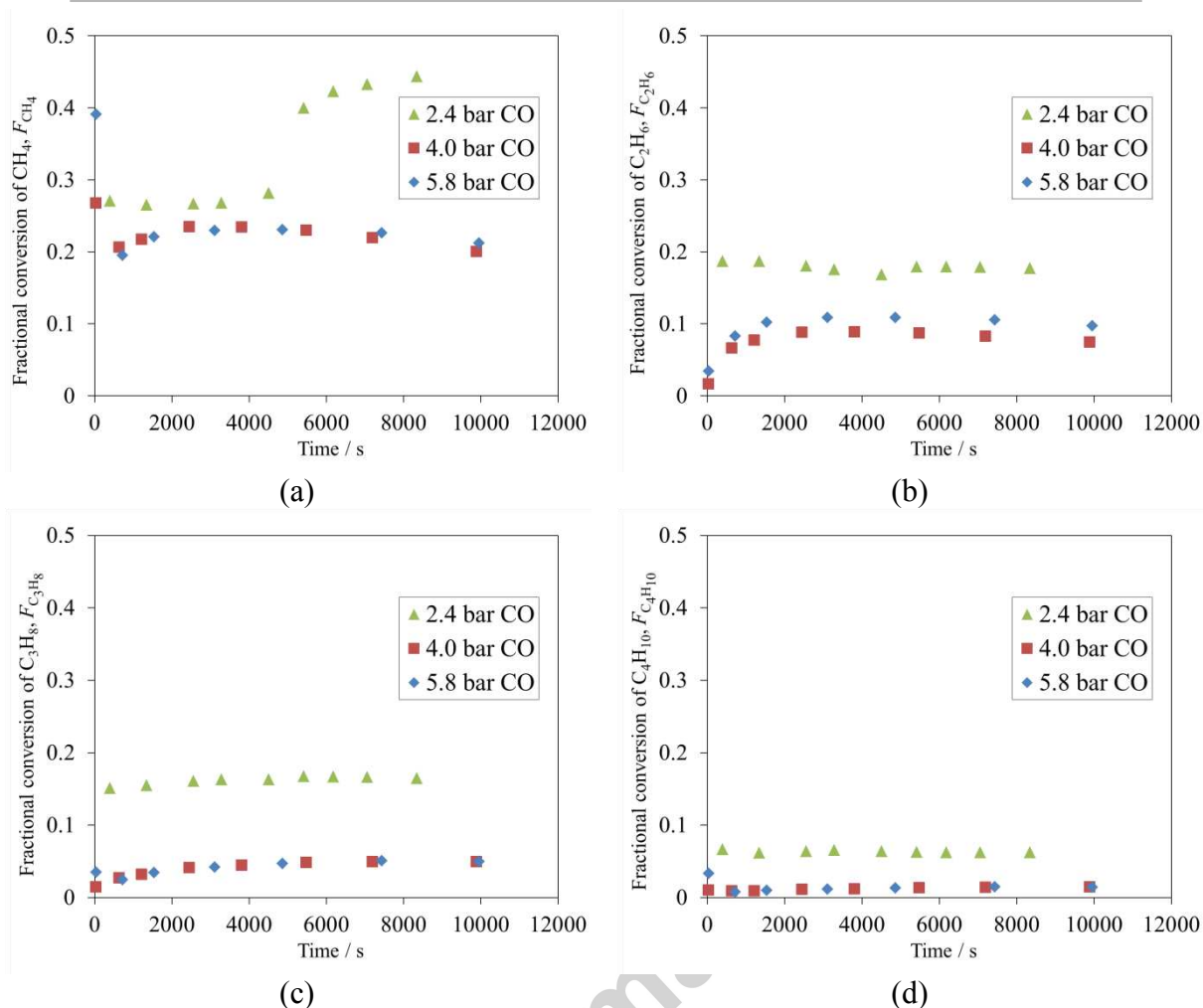


Figure 10. Fractional conversion of (a) CH_4 , (b) C_2H_6 , (c) C_3H_8 and (d) C_4H_{10} vs. partial pressure of CO consumed, for different initial partial pressures of CO. $p_{\text{H}_2,0} = 7.2$ bar, $T = 463$ K, $m_{\text{cat}} = 5.0$ g.

3.4 Effect of p_{CH_4} and p_{CO_2}

The effect of CH_4 on the rate and selectivity was explored by measuring the variation of partial pressure of H_2 , CO , CH_4 and CO_2 over time for different initial partial pressures of CH_4 , from 0 to 6 bar, at 463 K. The results, described in Supplementary Information Section 3, indicated there was no significant effect of p_{CH_4} on the rate of reaction and also that the product distribution was not affected by the introduction of additional p_{CH_4} . Thus, CH_4 behaved as a spectator molecule.

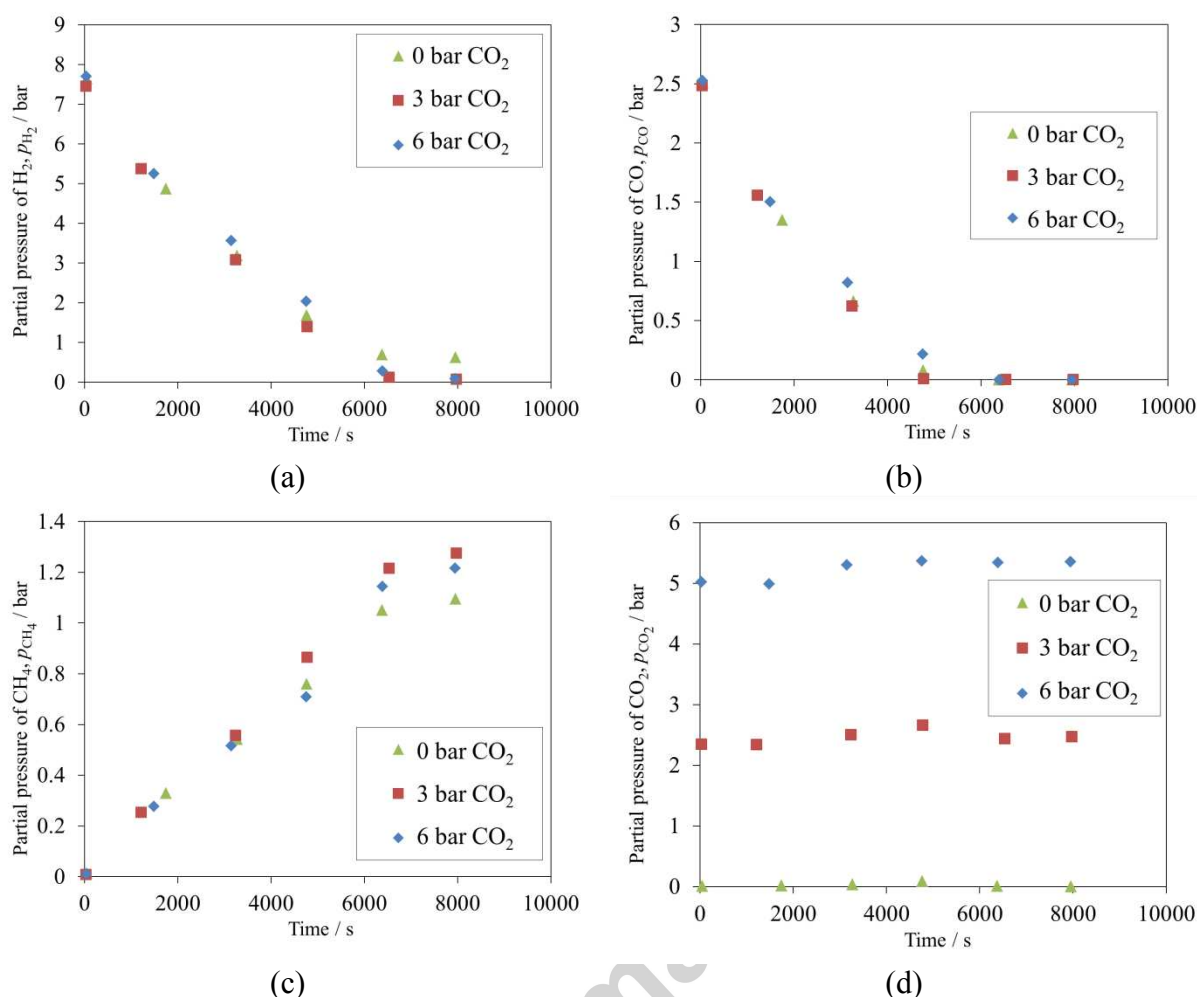


Figure 11. Variation of partial pressure of (a) H₂, (b) CO, (c) CH₄ and (d) CO₂ over time for different initial partial pressures of CO₂. $p_{\text{CO}_2,0} = 2.4 \text{ bar}$, $p_{\text{H}_2,0} = 7.2 \text{ bar}$, $T = 463 \text{ K}$ and $m_{\text{cat}} = 5.0 \text{ g}$.

To study the effect of CO₂, the reactor was first raised to the desired pressure with pure CO₂ before the mixture of CO and H₂ was introduced. The initial rates of reactions were identical for all different initial partial pressures of CO₂, $p_{\text{CO}_2,0}$ considered (0, 3 and 6 bar) as shown by the overlapping points in Figures 11 (a), (b) and (c) for $t < 4000 \text{ s}$. In all experiments, the transition from period I to II occurred at approximately the same time, $t \approx 5000 \text{ s}$. However, it is noted that p_{CH_4} differed after the transition from period I to II, i.e. at $t > 5000 \text{ s}$. At $t = 8000 \text{ s}$, p_{CH_4} increased from 1.1 bar when $p_{\text{CO}_2,0} = 0$ to $\sim 1.2 \text{ bar}$ for $p_{\text{CO}_2,0} = 3 \text{ bar}$. These observations suggest that H₂ reacted with CO during period I, and that following the depletion of p_{CO} , the remaining H₂ reacted with CO₂, resulting in the overall increase in p_{CH_4} at the end of the experiment. This is also consistent with the decrease of p_{CO_2} at $t > 5000 \text{ s}$, as shown in Figure 11 (d). The product distribution of the reaction was also not affected by the presence of CO₂ (results given in Supplementary Information Section 3). The

marked increase in p_{CH_4} during period II is therefore attributed to the production of additional CH_4 from CO_2 methanation.

3.5 Effect of $p_{\text{H}_2\text{O}}$

The effect of $p_{\text{H}_2\text{O}}$ was studied by first performing CO_2 methanation from a known initial pressure of CO_2 and H_2 in order to form CH_4 and H_2O , followed by the introduction of 2.4 bar of CO and 7.2 bar of H_2 . According to the stoichiometry of CO_2 methanation, the mixture of CO_2 and H_2 yielded, at the end of the reaction, a mixture of mainly CH_4 and H_2O with some excess CO_2 . It is important to note that no significant amounts of H_2 remained at the end of the CO_2 methanation reaction, before the introduction of CO and H_2 . This is because p_{H_2} has been shown, above, to have a significant influence on the rate and selectivity of methanation. The time, t , at which the mixture of CO and H_2 was introduced into the reactor was taken as $t = 0$ s. Since it has already been established that p_{CO_2} and p_{CH_4} have no effect on the rate and the selectivity of the reaction in the presence of CO , any effects observed could be attributed to the presence of H_2O . The effect of $p_{\text{H}_2\text{O}}$ was explored for temperatures 453 – 473 K. For the range explored up to $p_{\text{H}_2\text{O}} = 1.44$ bar, there were no effects on the rate of reaction and also the addition of $p_{\text{H}_2\text{O}}$ had very little effect on the product distribution of the reaction (results shown in Supplementary Information Section 4).

3.6 Effect of temperature

The effect of temperatures from 443 to 473 K on the rate of CO methanation reaction was studied using the reference initial condition of $p_{\text{CO},0} = 2.4$ bar and $p_{\text{H}_2,0} = 7.2$ bar. The variations of the partial pressures of H_2 and CO with time are illustrated in Figure 12. In general, the rate of reaction doubled for every increase in temperature of 10 K. This can be observed from the profile of p_{H_2} and p_{CO} in Figures 12 (a) and (b), where the time taken for p_{CO} to be depleted decreased by approximately 50% for every increase of 10 K. The rate of production of CH_4 also followed a similar trend. The transition from period I to II, noted by a marked increase in p_{CH_4} , was found to occur at all temperatures explored, as illustrated in Figure 13(a). This was also accompanied by the initial accumulation of CO_2 , followed by a fast consumption after the transition to period II when $p_{\text{CO}} = 0$, as shown in Figure 13 (b).

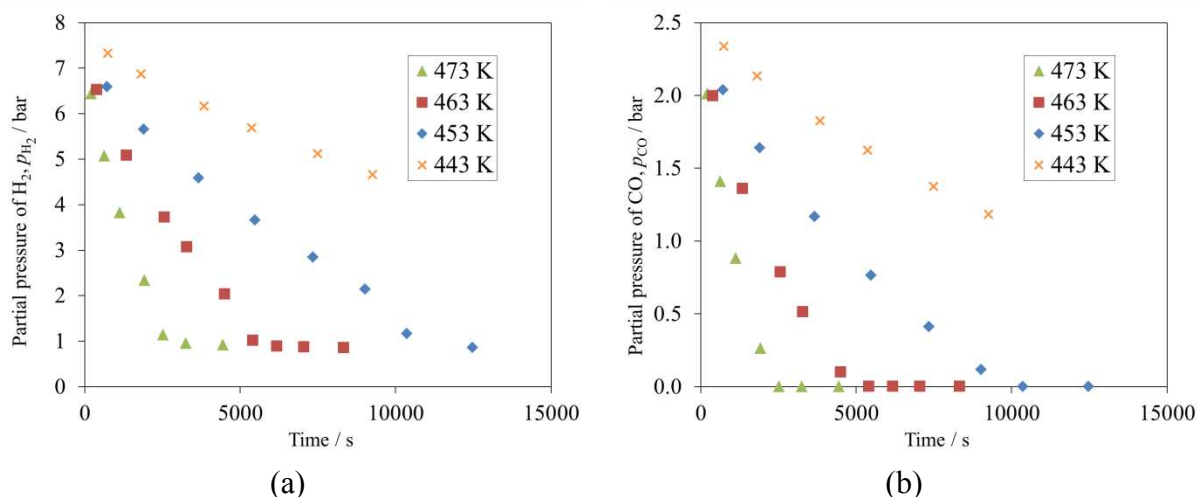


Figure 12. The partial pressure of (a) H₂ and (b) CO with time for different reaction temperatures. In all experiments, $p_{\text{CO},0} = 2.4 \text{ bar}$, $p_{\text{H}_2,0} = 7.2 \text{ bar}$ and $m_{\text{cat}} = 5.0 \text{ g}$.

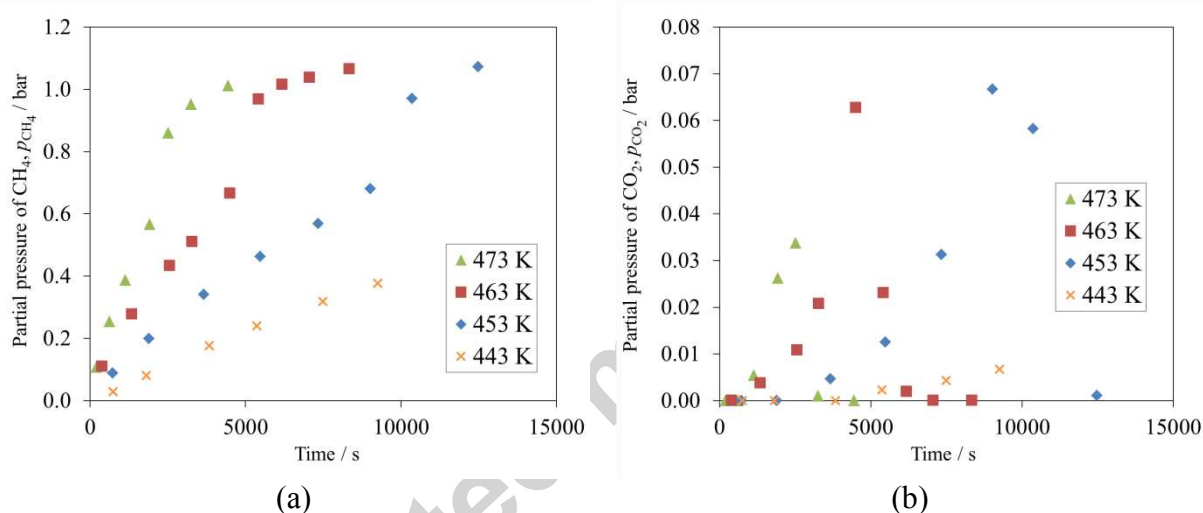


Figure 13. The partial pressure of (a) CH₄ and (b) CO₂ with time for different reaction temperatures. In all experiments, $p_{\text{CO},0} = 2.4 \text{ bar}$, $p_{\text{H}_2,0} = 7.2 \text{ bar}$ and $m_{\text{cat}} = 5.0 \text{ g}$.

It is interesting to note that the selectivity of the reaction was not affected by temperature. Results, shown in the Supplementary Information Section 5, indicated that the fractional conversion to CH₄ remained approximately constant at 0.26 within period I and increased to about 0.44 after the transition to period II, i.e. after the depletion of CO. The fractional conversions to other hydrocarbons were also found to be unchanged for the temperature range explored. Therefore, it can be concluded that the selectivity of the reaction was not a strong function of temperature, for temperatures 443 – 473 K, and that temperature only has an effect on the overall rate of reaction.

3.7 Temperature-programmed studies

Following CO methanation in the Carberry reactor, the spent catalyst was kept in a sealed glass jar after its removal from the reactor, after the final reaction – the methanation of CO₂ – had been conducted. During the transfer from the reactor, the nickel on the catalyst would have been partially oxidised by atmospheric oxygen and some of the weakly adsorbed species would have left the surface of the catalyst. The spent catalyst was subsequently subjected to temperature-programmed studies using the CATLAB apparatus. In an experiment, 50 mg of spent catalyst was placed in the quartz, tubular reactor and then subjected to a temperature programme whilst gases of various, fixed composition were passed through the packed bed of catalyst in the reactor. In all studies, the catalyst was subjected to a flowrate of the chosen gas mixture of 40 ml/min (at room temperature and pressure) at 120°C for 1 hour before the temperature was increased at a linear rate of 10°C/min. Different gases were used during the temperature ramp: Figure 14 shows the temperature programmed desorption (TPD) with a flow of 40 ml/min (at room temperature and pressure) of He, Figure 15 the temperature-programmed hydrogenation (TPH) in a flow of 40 ml/min (at room temperature and pressure) of a mixture of 5 vol% H₂ in He and Figure 16 the temperature programmed oxidation (TPO) with a flow of 5 ml/min (at room temperature and pressure) of O₂ and 35 ml/min (at room temperature and pressure) of He.

The TPD results show the evolution of H₂, CO₂, CO and CH₄ in two main regions; a sharp, narrow peak at 200°C and a broad peak ranging from 300 to 500°C. The evolution of water, illustrated in Figure 14 (b) shows two broad peaks, probably the result of some moisture on the catalyst as well as the possible reduction of nickel oxide by adsorbed H₂ or hydrocarbons. The evolution of carbon dioxide shows some interaction between the adsorbed carbon species with nickel oxide. It also demonstrates the presence of carbonaceous species on the surface of the catalyst during CO methanation. The TPH shows the evolution of CO₂, CO and CH₄ at about 200°C, illustrated in Figure 15. Broad peaks for CO₂ and CH₄ were also observed at a higher temperature of 280 – 500°C. However, no evolution of CO was observed within this temperature range. Compared to the TPD, the broad peaks for CO₂ and CH₄ at the higher temperatures appeared to start at a lower temperature in the hydrogenation experiment. This suggests that the carbonaceous material on the surface of the catalyst was more easily removed by reacting with H₂ than in an atmosphere of helium. It is also noted that the profile of H₂O evolution shown in Figure 15(b) is similar to that of the temperature-programmed

reduction of the passivated catalyst, which is unsurprising given that some of the catalyst would have been partially oxidised after its removal from the Carberry reactor.

In the TPO in Figure 16, CO₂ and CO were detected over a wide range of temperatures, ranging from 120 to 500°C. No significant CH₄ was observed over the duration of the experiment, as seen by its complete absence in both Figure 16(a) and (b), suggesting that most adsorbed carbonaceous species were oxidised directly to CO₂. Since the profiles of CO₂ and CO followed the same pattern, it is likely that the profile of CO is the result of the mass spectrometer detecting the CO fragment which originated from CO₂. The profile of H₂O also followed a similar pattern, suggesting the combustion of hydrocarbons to form CO₂ and H₂O. These temperature-programmed studies show the presence of two main forms of carbon on the surface of the catalyst following CO methanation: one which could be reduced and hydrogenated at 200 – 300°C and another in the region of 300 – 500°C.

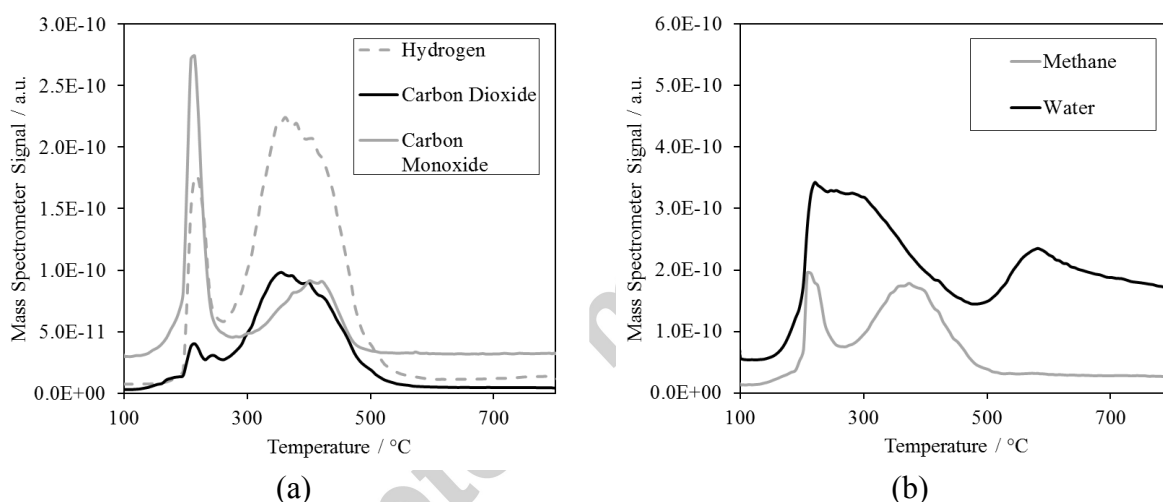


Figure 14. Temperature-programmed desorption using CATLAB on a spent Ni/ γ -Al₂O₃ catalyst after CO methanation in the Carberry reactor. A temperature ramp of 10°C/min was used. Signals of (a) hydrogen, carbon dioxide and carbon monoxide and (b) methane and water were plotted against temperature. The flow rate of He was 40 ml/min (at room temperature and pressure).

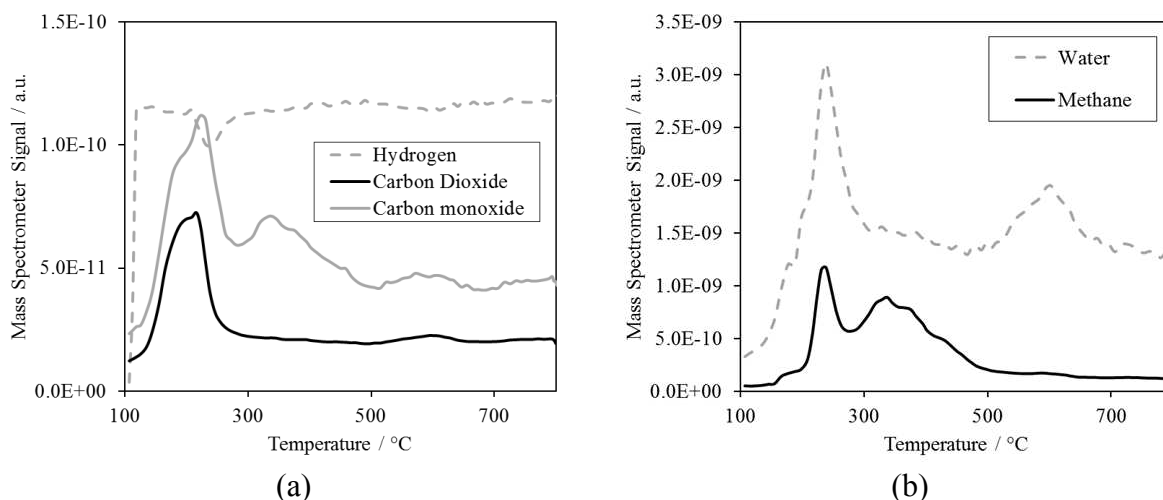


Figure 15. Temperature-programmed hydrogenation using CATLAB on a spent Ni/ γ -Al₂O₃ catalyst after CO methanation in the Carberry reactor. A temperature ramp of 10°C/min was used. Signals of (a) hydrogen, carbon dioxide and carbon monoxide and (b) methane and water were plotted against temperature. A flow rate of 40 ml/min (at room temperature and pressure) of a gas mixture of 5 vol% H₂ in He was passed through the catalyst bed.

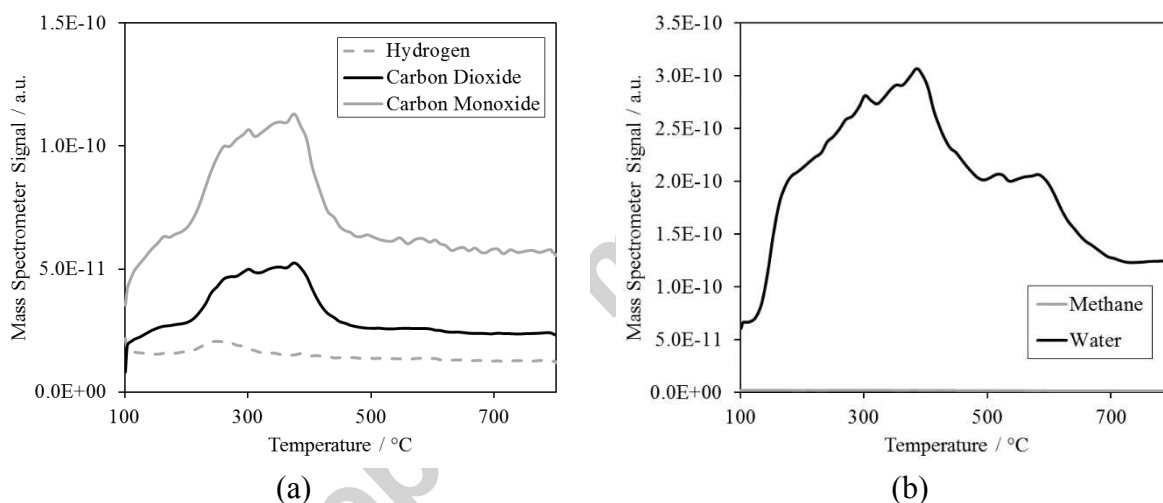


Figure 16. Temperature-programmed oxidation using CATLAB on a spent Ni/ γ -Al₂O₃ catalyst after CO methanation in the Carberry reactor. A temperature ramp of 10°C/min was used. Signals of (a) hydrogen, carbon dioxide and carbon monoxide and (b) methane and water were plotted against temperature. A flow rate of 5 ml/min (at room temperature and pressure) of O₂ and 35 ml/min of He (at room temperature and pressure) was passed through the catalyst bed. N.B. methane was below the limit of detection in (b).

The import of these observations is discussed in Section 5, below, after the modelling has been introduced and discussed.

3.8 DRIFTS measurements

The surface of the catalyst was probed using in-situ DRIFTS in which 50 mg of fresh, passivated 12 wt% Ni/ γ -Al₂O₃ catalyst was packed as a differential bed in the reactor

chamber and supported by a wire mesh. The catalyst was reduced at 450°C for 2 hours under 100 ml/min (at room temperature and pressure) of H₂. Following reduction, a mixture of 90 ml/min (at room temperature and pressure) of H₂ and 30 ml/min (at room temperature and pressure) of CO was introduced into the reaction chamber and passed through the differential bed. In-situ IR spectra were obtained at temperatures from 463 – 723 K. Figure 18 illustrates the main features of the IR spectrum obtained at 463 K at steady-state during CO methanation at atmospheric pressure. It is noted that the peaks at 2180 and 2120 cm⁻¹ in Figure 17 (a) are the result of the CO in the gas phase, which was confirmed with the reference IR spectrum of carbon monoxide. The presence of fringes around this region was attributed to the rotation of gas phase CO molecules. The peak at 2070 cm⁻¹ is the result of linear carbonyl groups on the surface of the catalyst. The large peaks at 1600, 1390, 1380 and 1330 cm⁻¹ in Figure 17 (a) can be attributed to formate groups. The peak at 2900 cm⁻¹ was also attributed to the presence of formate groups, as shown in Figure 17 (b).

Following CO methanation at 463 K, the stream of CO was turned off and only H₂ was passed through the catalyst bed. Spectrum (ii) in Figure 17 was obtained after 40 minutes in a flow of H₂ of 90 ml/min (at room temperature and pressure). The amount of carbonyl species, measured by the peak at 2070 cm⁻¹, decreased significantly. However, a significant quantity of carbonyl species were still present after 40 minutes in a flow of H₂, indicating a strong adsorption of CO on the surface of nickel. The intensity of the absorbance bands of the formate groups remained unchanged at the end of this period. This can be compared with CO₂ methanation (results shown in Supplementary Information Section 6) where the carbonyl groups disappeared completely after 40 minutes in H₂ whilst the formate groups experienced only a small decrease in intensity.

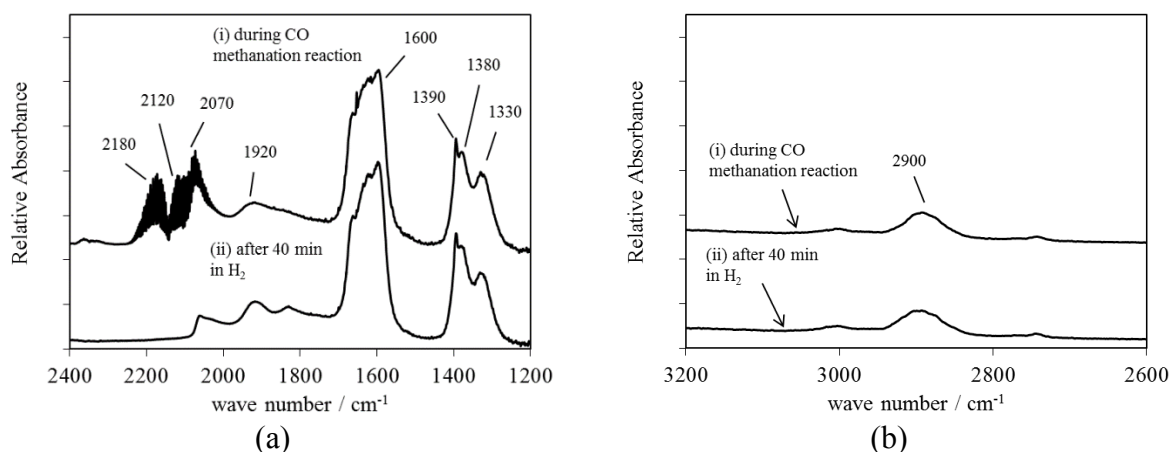


Figure 17. Infrared spectra of adsorbed species in the range of (a) 1200 – 2400 cm^{-1} and (b) 2600 – 3200 cm^{-1} formed on reduced 12 wt% Ni/ Al_2O_3 in a flow of (i) 90 ml/min (at room temperature and pressure) of H_2 and 30 ml/min (at room temperature and pressure) of CO and (ii) in 100 ml/min (at room temperature and pressure) of H_2 only, taken after 40 mins following the introduction of H_2 . The DRIFTS spectrum of the catalyst under He at 463 K was used as the background.

4. Theory

4.1 Reactor model

The batch reactor was modelled using the following set of ordinary differential equations, allowing for the water-gas shift reaction and the fact that the selectivity of the reaction towards CH_4 was only about 25% of the consumed CO:

$$\frac{dp_{\text{CO}}}{dt} = \frac{m_{\text{cat}} RT}{V_{\text{reactor}} \times 10^5} (-r_1' - r_2') \quad (6)$$

$$\frac{dp_{\text{H}_2}}{dt} = \frac{m_{\text{cat}} RT}{V_{\text{reactor}} \times 10^5} (-\alpha r_1' + r_2') \quad (7)$$

$$\frac{dp_{\text{CH}_4}}{dt} = \frac{m_{\text{cat}} RT}{V_{\text{reactor}} \times 10^5} (-\beta r_1') \quad (8)$$

$$\frac{dp_{\text{H}_2\text{O}}}{dt} = \frac{m_{\text{cat}} RT}{V_{\text{reactor}} \times 10^5} (r_1' - r_2') \quad (9)$$

$$\frac{dp_{\text{CO}_2}}{dt} = \frac{m_{\text{cat}} RT}{V_{\text{reactor}} \times 10^5} r_2', \quad (10)$$

Here r_1' is the rate of CO methanation, r_2' is the rate of the water-gas shift reaction, α is the consumption ratio of H_2 to CO in reaction r_1' and β is the fractional conversion of CO of

CH₄. The value of α is an average of the stoichiometric ratio of H₂ to CO based on the relative rates of Reactions (1) and (4). In the foregoing, the value of β was found to be constant for temperatures 453 – 473 K, but to be a strong function of the ratio of H₂ to CO. The fractional conversion of CO to CH₄ was also found to be largely constant during period I, viz. before the depletion of CO. A linear correlation for β was estimated as a function of the ratio of the initial partial pressure of H₂ to CO. The line of best fit had a gradient of 0.044 ± 0.008 , intercepting the ordinate at 0.16 ± 0.03 , where the uncertainty represents a 95% confidence interval. A correlation coefficient of 0.91 was obtained. This correlation was used to estimate the value of β in the solution of the above equations. It can also be assumed that Reactions (1) and (4) were the two main reactions during the reaction. Therefore, the consumption ratio of p_{H_2} to p_{CO} , α , was estimated using

$$\alpha = 3\beta + 2(1 - \beta). \quad (11)$$

Equations (6) to (11) were solved using the initial conditions of the experiments, i.e.

$$\text{for } t = 0, \quad p_i = p_{i,0}. \quad (12)$$

where p_i is the partial pressure of component i in bar and $p_{i,0}$ is the initial partial pressure of species i . Given suitable rate expressions for r_1' and r_2' , the equations were solved using the MATLAB solver ode45 to give the variation of the partial pressures of CO, H₂, CH₄, H₂O and CO₂ with time, for comparison directly with the experimental measurements.

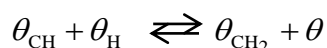
4.2 Kinetic modelling

This Section investigates different expressions for the rate of CO methanation, represented by r_1' in the above equations, using a Langmuir-Hinshelwood approach. The active sites for the reaction were assumed to be identical and their distribution uniform throughout the catalyst pellets. Extra-particle and intra-particle transport effects were taken to be absent. Four kinetic models are listed in Table 2. For Models I to III, it was assumed that CO methanation proceeded via the dissociative adsorption of CO with a sequence of steps:

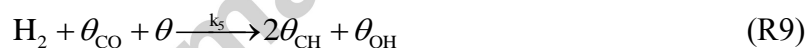




where k_i and k_{-i} are the forward and reverse rates of reaction of the specified elementary step. Further steps include hydrogenation of the θ_C and the subsequent desorption of θ_{CH_4} to form CH_4 in the gas phase. This involves a succession of steps of the form:



Three rate expressions, Eqs. (13) to (15) were derived based on different rate limiting steps and the most abundant surface species, given in Table 2. Model IV assumed an Eley-Rideal mechanism, where the rate-limiting step was taken as the reaction between gaseous H_2 and adsorbed CO, i.e.



It is reasonable to assume that the surface of the catalyst is saturated with adsorbed CO species in order for such a scenario to be feasible. Hence eq. (16) in Table 1. Three rate expressions for CO methanation, proposed by different investigators, are given in Table 2.

4.3 Model discrimination

It is obvious that not all the expressions given in Table 1 agree with the experimental results. Equation (14) predicts the rate of reaction to increase with p_{CO} and decrease with p_{H_2} , contrary to the experimental measurements, where the rate of reaction was found to increase with p_{H_2} and decrease with p_{CO} . The same argument could be applied to Eq. (15). Therefore, Eqs. (14) and (15) were not considered for further study. The rate expression proposed by van Herwijnen et al. (1973) predicted that the rate of reaction would decrease with p_{CO} at high values of p_{CO} . However, they did not account for the effect of p_{H_2} . Sughrue and Bartholomew (1982) proposed Eq. (19) with the assumption that the rate-limiting step of the reaction was different at different temperatures. At temperatures below 525 K, Eq. (19)

collapses to Eq. (13). Since all the experiments performed in this study were below 500 K, only Eq. (13) will be considered. There is some similarity between Eqs. (17) and (16), discussed later. Van Ho and Harriott (1980) derived Eq. (17) based on a Langmuir-Hinshelwood model with reaction between adsorbed carbon monoxide and hydrogen atoms.

Table 1. Kinetic rate expressions based on different assumptions of the rate limiting step and the most abundant surface species. p_i is the partial pressure of component i .

Model	Rate expression	Rate-limiting step	Most abundant surface species	
I	$\frac{a_I p_{H_2}}{(1 + b_I p_{CO})^2}$	Adsorption of H_2	CO	(13)
II	$\frac{a_{II} p_{CO}}{(1 + b_{II} \sqrt{p_{H_2}})}$	Adsorption of CO	H	(14)
III	$\frac{a_{III} p_{CO}}{(1 + b_{III} p_{CO} + c_{III} \sqrt{p_{H_2}})^2}$	Dissociation of CO	CO and H	(15)
IV	$\frac{a_{IV} p_{H_2} p_{CO}}{(1 + b_{IV} p_{CO})^2}$	Reaction of H_2 with adsorbed CO	CO	(16)

Table 2. Kinetic rate expressions proposed by different studies for CO_2 methanation.

Rate expression	Reference	
$r' = \frac{k p_{CO} p_{H_2}}{(1 + K_{CO} p_{CO} + K_{H_2} p_{H_2})^2}$	Van Ho and Harriott (1980)	(17)
$r' = \frac{k p_{CO}}{(1 + K_{CO} p_{CO})^2}$	van Herwijnen et al. (1973)	(18)
$r' = \frac{k p_{H_2}}{k_1 (1 + K_{H_2}^{0.5} p_{H_2}^{0.5} + K_{CO} p_{CO})^2 + k_2 (1 + K_{CO} p_{CO})^2}$	Sughrue and Bartholomew (1982)	(19)

Since the two most plausible rate expressions are Models I and IV, further comparison of these was performed by substituting the rate expressions into the model of the reactor, and comparing the agreement between theory and experiment at different conditions. To do this, the parameters for each model were estimated based on a least-squares minimisation. Thus, the agreement between model and experiment was studied by comparing the solution of the system of ODEs with the measured temporal variation of the partial pressures of the various species. In the minimisation, the difference, $d_i(t)$, between these values was compared for each iteration at time t with the experimental measurements for p_{CO_2} , p_{H_2} and p_{CH_4} :

$$d_i(t) = p_{i,\text{model}}(t) - p_{i,\text{exp}}(t) \quad (20)$$

where $p_{i,\text{model}}(t)$ is the partial pressure of species i determined by the solution of the ODEs and $p_{i,\text{exp}}(t)$ is the partial pressure of species i measured experimentally. The sum of all the squares of each component was evaluated at a given time, t , such that

$$D = \sum_i (d_i(t))^2. \quad (21)$$

Values of the parameters in the model were obtained by minimising D using the MATLAB routine `lsqnonlin`. Parameters were estimated using only the kinetic measurements in period I of the experiments, viz. for $p_{\text{CO}} > 0.1$ bar. During this process, rate expressions for Models I and IV were substituted into r_1' of Eqs. (6) to (10) while a rate expression for the water-gas shift reaction (Lim et al. 2016) was substituted into r_2' , i.e.

$$r_2' = \frac{a_{\text{WGS}} P_{\text{H}_2\text{O}} P_{\text{CO}}}{(1 + b_{\text{WGS}} P_{\text{CO}})}. \quad (22)$$

In general, the solution of Eqs. (6) to (10) was insensitive to values of r_2' because the maximum fractional conversion of CO to CO₂ is only $\sim 0.02 - 0.05$. Therefore, a_{WGS} was determined empirically at each temperature before the least-squares minimisation was performed. Values of a_{WGS} about 20% of those obtained by Lim et al. (2016) were found to agree with the experimental measurements of p_{CO_2} with time.

4.3.1 Model I

Model I was first proposed by Sughrue and Bartholomew (1982) for CO methanation for temperatures below 525 K. They performed continuous experiments on monolithic catalysts

using an internal recycle reactor. Since their experiments were performed in a continuous reactor, the batch method developed here offered an opportunity to compare techniques. Figure 18 illustrates the result using Model I for CO methanation and the experimental results obtained at 453 K for different initial partial pressures of H₂.

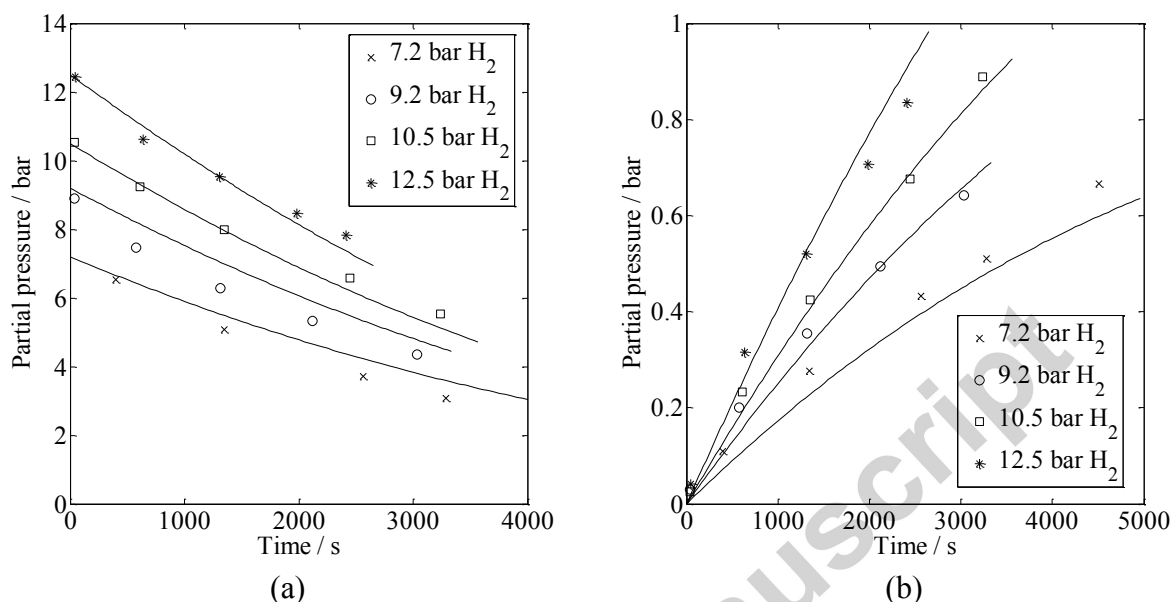


Figure 18. Comparison between the modelling results and the experimental results for different initial partial pressures of H₂. (a) shows the partial pressure of H₂ with time and (b) the partial pressure of CH₄ with time. $T = 453$ K, $p_{\text{CO},0} = 2.4$ bar and $m_{\text{cat}} = 5.0$ g. Solid lines are the predictions of Model I. The symbols represent experimental results with different initial partial pressures of H₂.

Figure 19 compares the modelling and experimental results at 473 K for different initial partial pressures of CO. In general, the model was capable of predicting a fairly constant rate of reaction during period I of the reaction. The kinetic parameters for Model I, a_1 and b_1 , at different temperatures are tabulated in Table 3. It is noted that b_1 represents a measure of the equilibrium constant between adsorbed and gaseous CO. In general, the predicted values of b_1 were found to be approximately constant over the range 443 – 473 K. However, the values obtained in Table 3 were very much larger than those reported by other studies. For a temperature of 463 K, the value of b_1 was 22 bar⁻¹, based on the extrapolation of the measurements by Sughrue and Bartholomew (1982); Huang and Richardson (1978) gave $b_1 = 74$ bar⁻¹. However, the reported values of b_1 by these researchers were based on experiments at temperatures > 523 K, significantly higher than those in the present work.

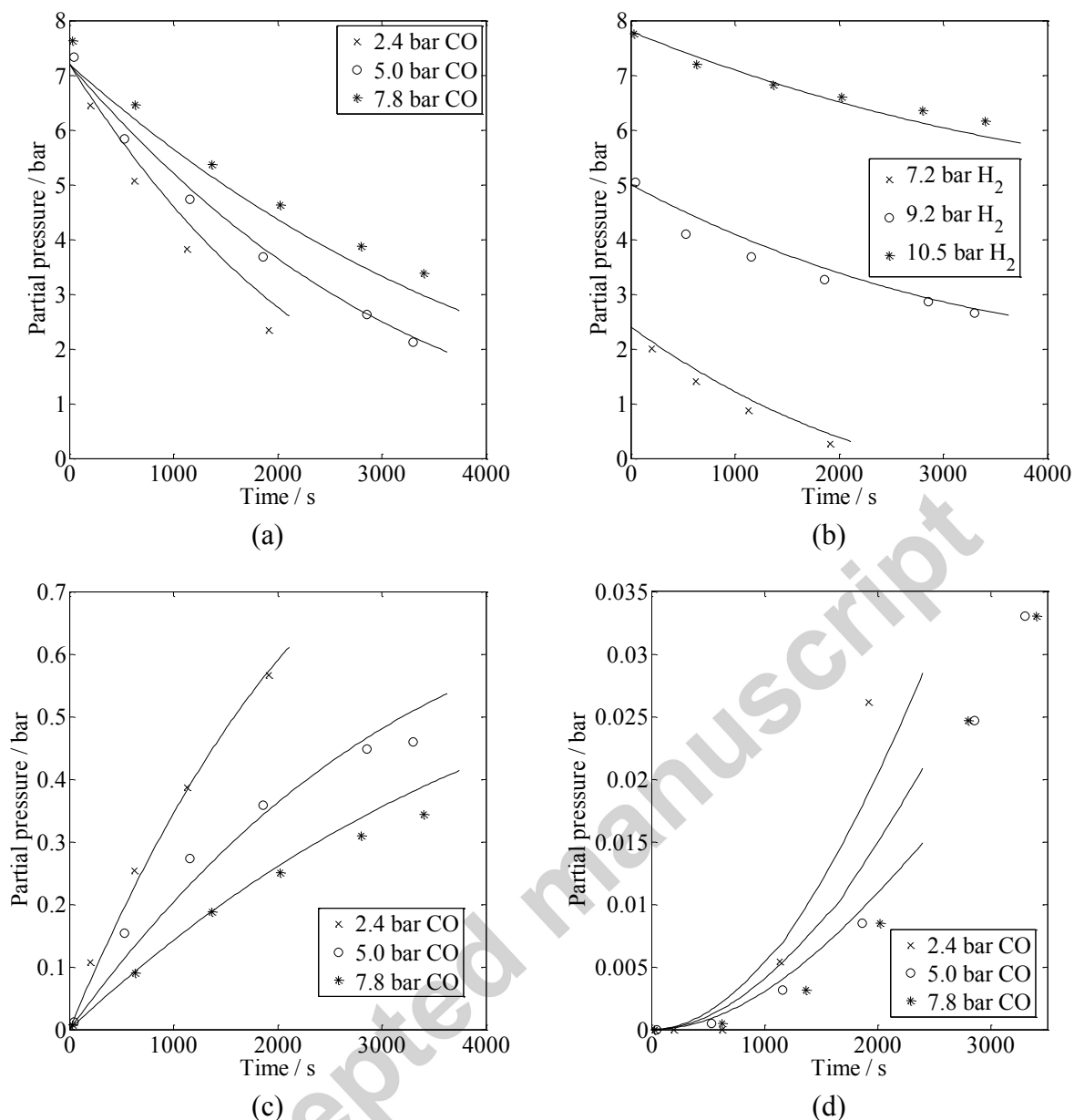


Figure 19. Comparison between the modelling results and the experimental results for different initial partial pressures of CO. The partial pressure of (a) H_2 , (b) CO, (c) CH_4 and (d) CO_2 are plotted against time. $T = 473$ K, $p_{CO,0} = 2.4$ bar and $m_{cat} = 5.0$ g. The solid lines are the predictions of Model I. The symbols represent experimental results for different initial partial pressure of CO.

Table 3. Values of the kinetic constants from the least-squares fit of Model I with the experimental results.

Temperature / K	$a_1 / \text{mol s}^{-1} \text{kg}^{-1}$	b_1 / bar^{-1}
443	$(3.4 \pm 0.2) \times 10^{-6}$	0.16 ± 0.05
453	$(4.2 \pm 0.2) \times 10^{-6}$	0.05 ± 0.02
463	$(9.8 \pm 0.5) \times 10^{-6}$	0.05 ± 0.01
473	$(2.2 \pm 0.1) \times 10^{-5}$	0.07 ± 0.01

4.3.2 Model IV

The agreement between the experimental measurements and the modelling results, using Model IV for the rate of CO methanation, is illustrated in Figures 20 and 21. It is clear that there is good agreement between theory and experiment. Model IV predicts a deceleration of the rate of reaction towards the end of period I of the reaction, so that the variation of p_{H_2} with time appeared to level off at $t > 2000$ s in Figure 20 (a). A similar behaviour was found in Figure 20 (b), which illustrates the variation of p_{CH_4} with time. The values of b_{IV} , which also represents a measure of the equilibrium constant between adsorbed and gaseous CO, are given in Table 4. It was found that, as with Model I, there was very little variation in the values of b_{IV} obtained from the least-squares minimisation at different temperatures. While the values of b_{IV} were an order of magnitude larger than those obtained for b_1 , they were still significantly smaller than those reported in the literature.

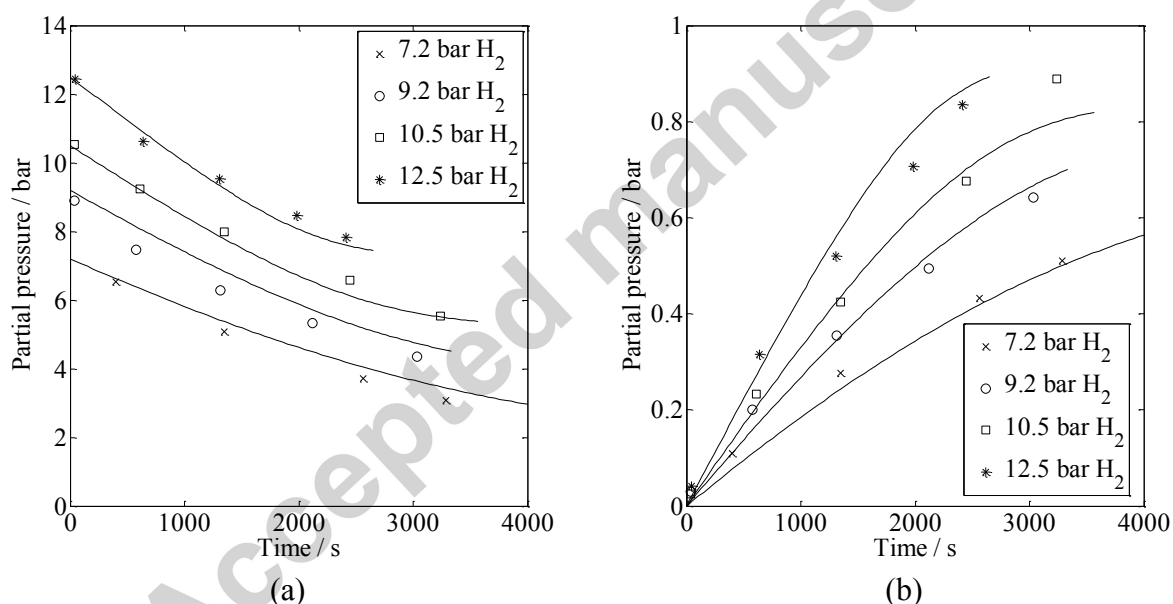


Figure 20. Comparison between the modelling results and the experimental results for different initial partial pressures of CO. (a) shows the partial pressure of H₂ with time and (b) the partial pressure of CH₄ with time. $T = 463$ K, $p_{\text{CO},0} = 2.4$ bar and $m_{\text{cat}} = 5.0$ g. The solid lines are the predictions of Model IV. The symbols represent experimental results for different initial partial pressure of CO.

Table 4. Kinetic constants from the least-squares fit of Model IV with the experimental results.

Temperature / K	$a_{\text{IV}} / \text{mol s}^{-1} \text{kg}^{-1}$	$b_{\text{IV}} / \text{bar}^{-1}$
443	$(8.0 \pm 0.2) \times 10^{-6}$	0.93 ± 0.03
453	$(1.3 \pm 0.1) \times 10^{-5}$	0.90 ± 0.10
463	$(3.2 \pm 0.2) \times 10^{-5}$	0.87 ± 0.04
473	$(8.0 \pm 0.3) \times 10^{-5}$	0.96 ± 0.02

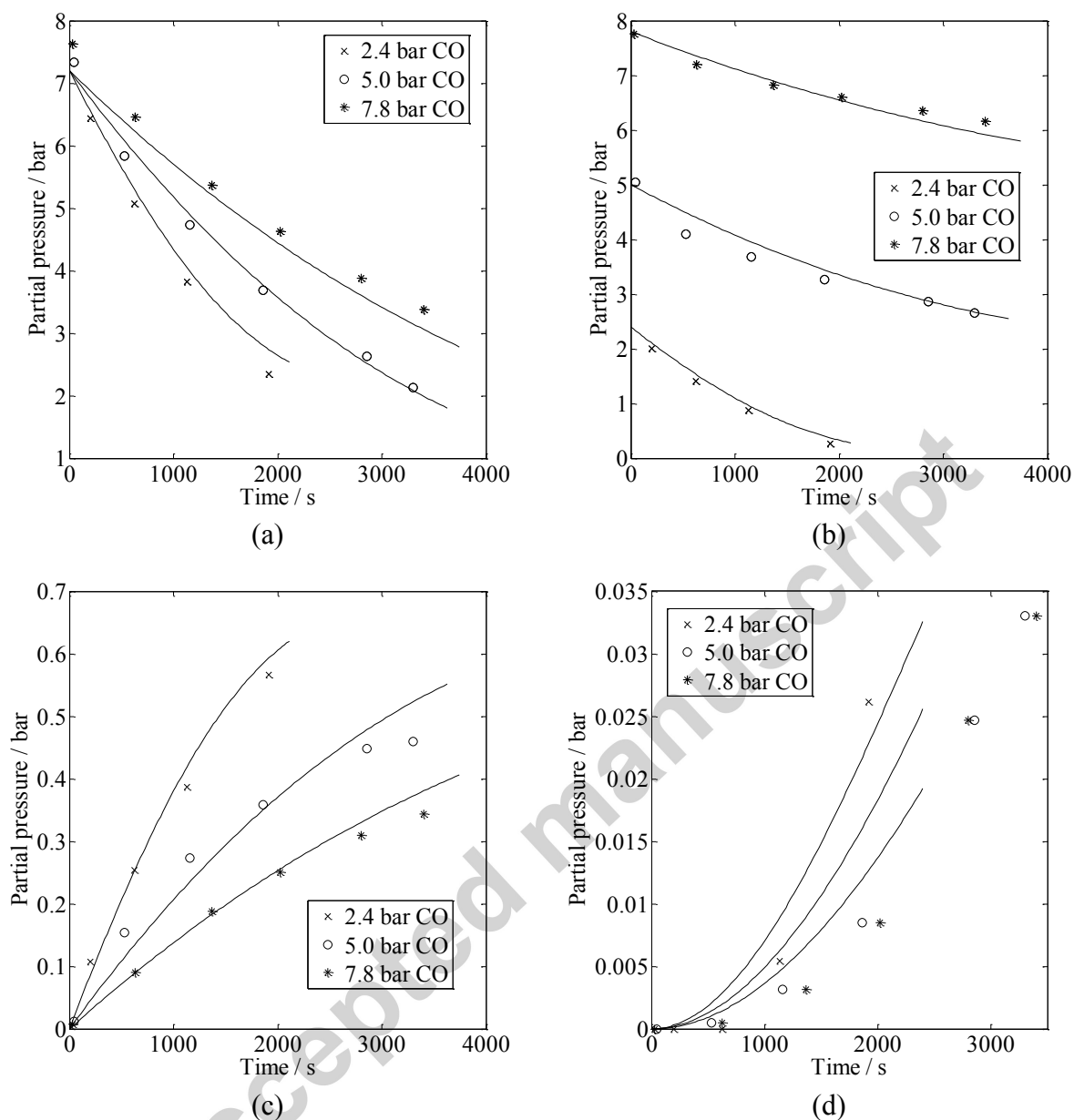


Figure 21. Comparison between the modelling results and the experimental results for different initial partial pressures of CO. The partial pressure of (a) H_2 , (b) CO, (c) CH_4 and (d) CO_2 are plotted against time. $T = 473\text{ K}$, $p_{H_2,0} = 7.2\text{ bar}$ and $m_{cat} = 5.0\text{ g}$. The solid lines are the modelling the predictions of Model IV. The symbols represent experimental results for different initial partial pressure of CO.

5 Discussion

Figures 2 (a) and (b) clearly show a transition in the behaviour of the reaction when p_{CO} approached zero. When significant p_{CO} was present in the gas phase, the rate of reaction was found to be almost constant, as observed by the linear increase in p_{CH_4} with time. When p_{CO} approached zero, the rate of production of p_{CH_4} was found to increase significantly, as

illustrated by the large rise in p_{CH_4} . This behaviour was not found in the partial pressures of higher hydrocarbons, such as C_2H_6 and C_3H_8 , and their partial pressures were found to be approximately unchanged after the amount of CO present fell to zero. Also, the total equivalent amount of carbon in the gas phase decreased steadily over time before the depletion of CO, suggesting the accumulation of carbon-containing species during this period which could not be accounted for by the sum of all the carbon-containing species in the gas phase. The nature of these species is speculated to be either liquid hydrocarbons in the pores of the catalyst or carbonaceous species on the surface of catalyst. It should be noted that CO adsorbed on the surface of the catalyst could also contribute to the consumption of CO from the gas phase. The recovery of the total carbon in the gas phase after the depletion of p_{CO} , i.e. during period II of the batch reaction, is probably attributable to the increase in the overall quantity of p_{CH_4} produced. The conversion of the CO_2 accumulated during period I to CH_4 was insufficient to account for the total amount of p_{CH_4} produced in period II since only a very small amount of p_{CO_2} was produced during period I. This suggests either the hydrogenation of carbonaceous species on the surface of the catalyst to form CH_4 or the production of CH_4 via hydrogenolysis of the higher hydrocarbons to form CH_4 , i.e. the splitting of higher hydrocarbons to light hydrocarbons. Ni catalysts are known to perform hydrogenolysis on longer-chain paraffins (Kikuchi and Morita, (1969). In fact, $\theta\text{-Al}_2\text{O}_3$ is active in the hydrogenolysis of cis-2-pentenenitrile (McGregor et al., 2010).

The values of p_{H_2} and p_{CO} had a significant influence on the rate and selectivity of the reaction. When p_{H_2} was increased, the rate of reaction increased and the selectivity towards CH_4 was greater. However, the selectivity towards other light paraffins remained relatively unchanged. The increased selectivity of the reaction towards CH_4 led to a higher proportion of carbon contained in the species in the gas-phase as illustrated in Figure 8. Conversely, when p_{CO} was increased, both the rate of reaction and the CH_4 selectivity decreased. Over the range 443 – 473 K, the fractional conversion of CO to CH_4 was found to range from 0.22 to 0.30. In general, this was found to be slightly lower than the values reported in the literature of about 0.4 – 0.7 % (Zhang et al., 2013; Fujita and Takezawa, 1997; Vance and Bartholomew, 1983). However, it is noted that the values of p_{CO} explored in this study were significantly larger than those used in investigations by other researchers. Therefore it is reasonable that the fractional conversion of CH_4 was slightly lower.

5.1 Comparison with CO₂ hydrogenation

The methanation of CO₂ over the 12 wt% Ni/ γ -Al₂O₃ catalyst in a batch reaction has been investigated by Lim et al. (2015). When a similar partial pressure of CO₂ and H₂ was introduced into the reactor in the presence of CO, the reaction was found to proceed via CO methanation instead of CO₂ methanation. This means that CO₂ behaves as a spectator molecule in the bulk gas phase and is not involved as a reactant in any reaction until the depletion of CO in the gas phase. This is consistent with Zhang et al. (2013), who studied CO methanation from 548 – 633 K and over a total pressure range of 1 to 5 bar in a continuous, fixed-bed reactor. They found no effect of CO₂ on the rate and selectivity of the reaction when 0.6 bar of CO₂ was co-fed with a mixture of 1.2 bar H₂ and 0.6 bar CO. This observation suggests that nickel has a much stronger affinity for CO compared to CO₂ and in the presence of CO, the surface of the catalyst preferentially adsorbs CO over CO₂. This has been confirmed by Inui et al. (1978), who found that the amount of CO adsorbed was nearly six times the amount of CO₂ adsorbed on a 5 wt% Ni/SiO₂ at 295 K.

Figure 22 compares the rates of production of CH₄ and the rates of consumption of CO and CO₂, in CO and CO₂ methanation reactions respectively, in the batch reactor. At 463 K, the initial rate of consumption of CO₂, for an initial condition of $p_{\text{H}_2,0} = 7.2$ bar and $p_{\text{CO}_2} = 2.4$ bar, was the same as the rate of consumption of CO when $p_{\text{H}_2,0} = 7.2$ bar and $p_{\text{CO}} = 2.4$ bar. However, the rates of production of CH₄ with time were very different. The CH₄ selectivity in CO₂ methanation was found to exceed 99.5%, which is significantly larger than that observed in CO methanation, with a value of only about 25%. When CO₂ methanation was performed, the rate of reaction decreased over time as a result of the decrease in the partial pressures of the reactants and no marked increases in the rate production of CH₄ were found on depletion of the CO₂, in contrast to the case with CO methanation during the transition from period I to II. The strong adsorption of CO on the surface of the catalyst suggests that the ratio of hydrogen to carbon on the surface is much lower than in CO₂ methanation, explaining the reduced selectivity for CH₄ in CO methanation.

The variation of the rate with temperature of CO methanation with temperature was found to be more sensitive than that of CO₂ methanation, as observed in Figure 22 (b). For a 10 K rise in temperature, the increase in the rate of consumption of CO, in CO methanation, was more than the increase in the rate of consumption of CO₂ in CO₂ methanation. This implies

that the apparent activation energy of CO methanation is different to that of CO₂ methanation, suggesting that the rate-limiting step is different in each case. This is consistent with the postulate that the rate-limiting step in CO₂ methanation is the dissociation of adsorbed CO while that in CO methanation is either the adsorption of H₂ or the reaction between gaseous H₂ and adsorbed CO. Having different rate-limiting steps for these processes is not unreasonable given that the surface of the catalyst is expected to be significantly different under different reaction conditions.

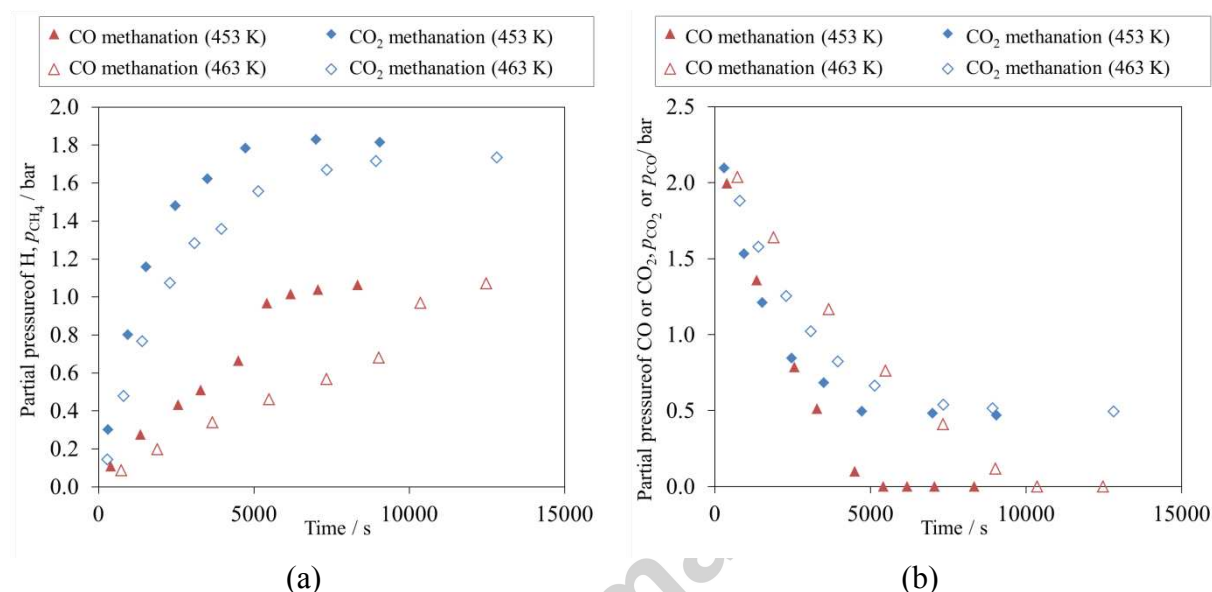


Figure 22. Partial pressure of (a) CH₄ and (b) CO or CO₂ with time at different temperatures for CO methanation and CO₂ methanation. The solid symbols represent the partial pressures of CH₄ and CO for initial conditions of $p_{\text{H}_2,0} = 7.2$ bar and $p_{\text{CO}} = 2.4$ bar. Open symbols represent the partial pressure of CH₄ and CO₂ for initial conditions of $p_{\text{H}_2,0} = 7.2$ bar and $p_{\text{CO}_2} = 2.4$ bar. The mass of catalyst $m_{\text{cat}} = 5.0$ g for all experiments.

The rate of CO₂ methanation decreased in the presence of $p_{\text{H}_2\text{O}}$ (Lim et al., 2015), but the results in the present paper show no such influence of H₂O in CO methanation. The literature suggests, however, that H₂O inhibits the rate of CO methanation (Zhang et al., 2013; Sughrue and Bartholomew, 1982). This conflict in observations is probably explained by the experiments in this paper being performed at temperatures significantly lower than those used in studies where inhibition occurred. It is likely that the low temperature, together with the strong adsorption of CO, led to little opportunity for the competitive adsorption of H₂O on the surface of the catalyst, which has been proposed as the primary method of inhibition of the rate in CO₂ methanation.

5.2 Nature of catalyst surface

Evidence for the presence of carbonaceous species on the surface of the catalyst or heavy hydrocarbons in the pores of the catalyst can be found in the measurements from temperature-programmed studies of the spent catalyst. That significant quantities of carbon-containing species were available on the surface of the spent catalyst is evident from the evolution of CO₂ in Figure 14 and CH₄ in Figure 15. The temperature-programmed studies also suggest two main forms of carbon based on the presence of two ranges of temperature in which CH₄ and CO₂ were evolved during the temperature programme. Kester and Falconer (1984) made similar observations and suggested that the CO was adsorbed on two different sites, i.e. one where nickel atoms are bonded to other nickel atoms, the other where there is a stronger interaction between nickel and the supporting material, i.e. Al₂O₃. This is consistent with the temperature-programmed reduction studies of the passivated catalyst, where two main regions of reduction of nickel were found. The presence of multiple active sites would also suggest that different processes are active at different temperature, which would lead to different kinetic expressions as suggested by Sughrue and Bartholomew (1982).

It is challenging to decide whether the presence of carbon-containing species on the surface of the catalyst is the result of adsorbed CO, liquid hydrocarbons or carbonaceous species on the surface from the existing evidence. Studies by Tottrop (1976) and Gardner and Bartholomew (1981) have shown that the rate of formation of carbon on the surface of the catalyst decreases in the presence of H₂ and H₂O, both of which were available in abundance for most of the duration of the batch reaction. By extrapolating the rate of carbon deposition observed by Gardner and Bartholomew (1981), where the mass of the catalyst was monitored under a flow of H₂ and CO, there is negligible formation of carbon at temperatures below 473 K. The origin of the carbon detected in the temperature-programmed studies is probably a combination of small quantities of liquid hydrocarbons in the pores and adsorbed CO.

The nature of the adsorbed CO was explored using DRIFTS. Significant amounts of bridge and linear carbonyl groups, as shown by the persistent absorbance bands at 2180 and 2120 cm⁻¹ in Figure 17 (a), are present on the surface of the catalyst. The decrease in the intensity of the carbonyl groups when the catalyst was subjected to pure H₂ at 463 K suggests that the hydrogenation of carbonyl groups was responsible for the evolution of CH₄ in the TPR profile of the spent catalyst at about 473 K. Furthermore, the intensities of bands assigned to the formate groups remained unchanged during the same period, suggesting that a higher temperature is required to hydrogenate these species. The evolution of additional CO₂

in the TPD and CH₄ in the TPR profiles is in good agreement with this observation. The decrease in the intensity of the carbonyl peaks after CO methanation was found to be slower than that after CO₂ methanation, which is expected given that the surface of the catalyst in CO methanation has been found to be much more heavily covered by carbonyl species compared to the case with CO₂ methanation. The IR spectra at temperature above 623 K were also found to be markedly different to those at lower temperatures, suggesting a possible change in the surface of the catalyst as the temperature was raised above 623 K.

5.3 Model comparison

It is difficult to discriminate between the two models based on the computer fitting of the models to the experimental results because both models gave reasonable agreement.

Model I assumes that the rate-limiting step is the adsorption of H₂ on the surface of the catalyst and that the surface of the catalyst is mainly adsorbed CO. This agrees with Sughrue and Barholomew (1982), who also observed that the reaction order for [H₂] was unity and that of [CO] was -1 at 475 K. However, the ranges of p_{CO} and p_{H_2} explored in Sughrue and Barholomew's (1982) studies (p_{CO} from 0.05 – 0.12 bar and p_{H_2} from 0.12 – 0.30 bar) were very low compared to those explored in this paper. However, it is interesting to note that the value of b_1 was very much smaller than that reported by Sughrue and Barholomew (1982).

Model IV was based on an Eley-Rideal mechanism. For this mechanism to be true, the surface of the catalyst must be saturated with CO. The evidence for this has already been discussed. However, it should be noted that a similar rate expression was derived by Van Ho and Harriott (1980), as given in Eq. (17). If the adsorption constant of H₂ is small, then Eq. (17) converges to Eq. (16). The derivation of Eq. (17) was based on a rate-limiting step involving the hydrogenation of adsorbed CO by two adsorbed H. It is impossible to discriminate between the two underlying mechanisms for the reaction of CO and H₂, highlighting the limitations of kinetic studies where different mechanisms could lead to the same rate expression. Nevertheless, it can be established that the strong adsorption of CO on the surface of the catalyst competes with H₂ for available active sites. It is also possible that H₂ adsorbs on different nickel sites to CO as a result of heterogeneity in the surface of the catalyst, as suggested by Andersson et al. (2008). The adsorbed hydrogen on different sites would replace the position of gaseous CO in the derivation of the Eley-Rideal mechanism to obtain the same expression. There also remains the possibility of the dissociated hydrogen migrating to the Al₂O₃ support, i.e. hydrogen-spillover, which occurs on nickel catalysts

supported on Al_2O_3 (Kramer and Andre, 1979; Gardes et al., 1974). The reaction between H on Al_2O_3 and CO on the nickel is also consistent with Model IV. Furthermore, the ability of Al_2O_3 to catalyse the hydrogenolysis of longer-chain hydrocarbons (McGregor et al., 2010) also suggests the presence of active sites on the supporting material.

Figure 23 shows the variation of the partial pressure of CO, H_2 , CH_4 and CO_2 as a function of time for an additional batch experiment with an initial condition of $p_{\text{CO},0} = 2.4$ bar and $p_{\text{H}_2,0} = 7.2$ bar at 463 K. At $t = 3600$ s, additional H_2 and CO were introduced in the ratio of 3:1. In general, both models were found to give good agreement with the experimental results, but both deviate from the experimental measurements at low p_{CO} . These models were derived on the assumption that the surface of the catalyst remains approximately constant over the length of the reaction. Since the relative quantities of adsorbed species on the surface of the catalyst is expected to change significantly as CO depletes, it is likely that values of the kinetic parameters also change during this period, which could be a limitation of the analysis. A change in the reaction mechanism as a result of the change in the amount of gaseous CO remains a possibility, suggesting that different rate expressions are valid for different p_{CO} . It can also be seen that the transition from period I to II was delayed when additional H_2 and CO was introduced at 3600 s. This is evident from the extension of the increase of p_{CH_4} at an approximately constant rate until the eventual depletion of CO when a marked increase in p_{CH_4} was observed. This experiment confirmed the need for CO to be depleted before carbon-containing species on the surface could be hydrogenated or adsorbed liquid hydrocarbons could undergo hydrogenolysis.

In both models, the increase in the rate of production of CO_2 was successfully reproduced by the rate expression for the water-gas shift reaction, Eq. (22), with the increase in $p_{\text{H}_2\text{O}}$ leading to an increase in the rate of reaction. Measuring the effect of p_{H_2} on the rate of the water-gas shift reaction independent of CO methanation is difficult because the introduction of H_2 to an initial mixture of H_2O and CO would lead to the consumption of CO by both the water-gas shift and CO methanation.

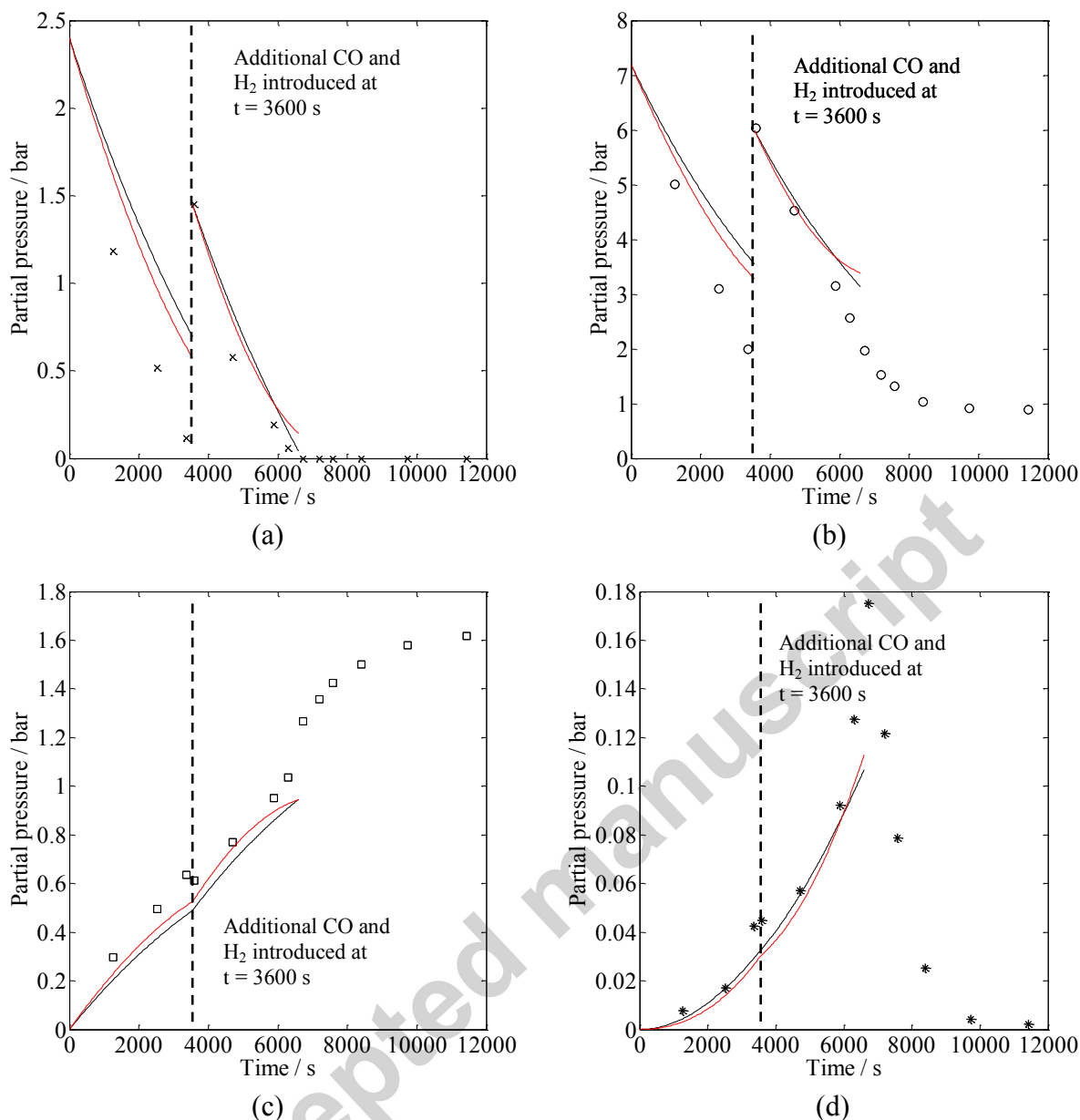


Figure 23. Comparison of the experimental results and the modelling results of Models I and IV. The partial pressures of (a) CO, (b) H₂, (c) CH₄ and (d) CO₂ were compared. At $t = 0$ s, $p_{\text{CO},0} = 2.4$ bar and $p_{\text{H}_2,0} = 7.2$ bar. Additional CO and H₂ were introduced at 3600 s. For all experiments, $T = 463$ K and $m_{\text{cat}} = 5.0$ g. The solid black line represents model I and the red line represents Model IV.

6 Conclusions

The conclusions were as follows:

- The rate of reaction of the CO methanation reaction and the selectivity of CH₄ was found to increase with p_{H_2} and decrease with p_{CO} .

- Two main regimes were identified over the length of the reaction in batch. In all experiments, the reaction initially proceeded with a constant rate period. This was followed by a marked increase in the rate of production of CH₄ after the depletion of p_{CO}. This increase in CH₄ was attributed to the hydrogenation of remaining carbonyl groups on the surface as well as the hydrogenolysis of long-chained paraffins in the reactor.
- The selectivity for CH₄ was found to be significantly lower than that observed in CO₂ methanation. This was found to be consistent with the low H₂ to CO ratio on the surface of the catalyst.
- Temperature-programmed studies performed on the spent catalyst identified two main types of carbonaceous species on the surface of the catalyst. These findings were correlated with the observations in the DRIFTS studies in order to postulate the presence of (i) carbonyl species on nickel clusters and (ii) formate groups on nickel sites which have a stronger interaction with the alumina support. The former was found to be reactive at the temperatures explored in this paper.
- The rate of CO methanation was insensitive to the presence of H₂O. This was attributed to the strong affinity of the nickel catalyst for CO, which saturates the surface of the catalyst leaving little opportunity for the adsorption of H₂O.
- The kinetic measurements were compared against the modelling predictions from several rate expressions. Equations (13) and (16) were both found to provide reasonable agreement with the experimental results. The derivation of Eq. (13) assumes the adsorption of H₂ to be the rate-limiting step while the rate-limiting step of Eq. (16) is the reaction of gaseous H₂ with adsorbed CO. The strong adsorption of CO on the surface of the catalyst, evident from various experimental observations, is consistent with both mechanisms. The agreement of these models was found to be less good towards lower p_{CO}, suggesting that the kinetic parameters or the rate mechanism could be a function of the CO coverage on the surface. However, it remains difficult to discriminate between the validity of Eqs. (13) and (16) with the existing experimental evidence.
- The production of CO₂ during the batch reaction of CO methanation was the result of the water-gas shift reaction.

Using a batch reactor, rather than a continuous one, for the study of CO methanation has certain advantages. The ability to observe intermediate products, such as CO₂, over the length of batch reaction has demonstrated the strong affinity of the nickel catalyst towards CO. Furthermore, the validity of different rate expressions, as well as the corresponding kinetic constants, was readily examined over a wide range of partial pressures using the batch reactor. The progress of CO₂ methanation and CO methanation in the batch reactor was significantly different, as a result of different rate-limiting steps and a significantly higher quantity of carbonyl groups on the surface of the catalyst in the case of CO methanation.

Acknowledgements

JYL was funded by the Cambridge International Scholarship Scheme. The Cambridge Philosophical Society, the Lundgren Research Award and Corpus Christi College are also gratefully thanked for contributing to the support of his PhD studies. We are grateful for the assistance of Dr A.P.E. York, Johnson Matthey Technology Centre, Sonning Common, Reading RG4 9NH, United Kingdom, for his valuable input to this research.

References

- Andersson, M. P., Abild-Pedersen, F., Remediakis, I. N., Bligaard, T., Jones, G., Engbæk, J. R. Sehested, J., Rostrup-Nielsen, J. R., Norskov, J. K., Chorkendorff, I. (2008). Structure sensitivity of the methanation reaction: H₂-induced CO dissociation on nickel surfaces. *Journal of Catalysis*, **255** (1), 6-19.
- Araki, M., Ponc, V. (1976). Methanation of carbon monoxide on nickel and nickel-copper alloys. *Journal of Catalysis*, **44** (3), 439-448.
- Chang, F. W., Hsiao, T. J., Chung, S. W., Lo, J. J. (1997). Nickel supported on rice husk ash—activity and selectivity in CO₂ methanation. *Applied Catalysis A: General*, **164** (1), 225-236.
- Clarke, A. W., Trinnama, J. A. (2010). *Survey of Energy Resources*. World Energy Council.
- Fujita, S. I., Nakamura, M., Doi, T., Takezawa, N. (1993). Mechanisms of methanation of carbon dioxide and carbon monoxide over nickel/alumina catalysts. *Applied Catalysis A: General*, **104** (1), 87-100.
- Fujita, S. I., Takezawa, N. (1997). Difference in the selectivity of CO and CO₂ methanation reactions. *Chemical Engineering Journal*, **68** (1), 63-68.
- Gardes, G. E. E., Pajonk, G. M., Teichner, S. J. (1974). Catalytic demonstration of hydrogen spillover from nickel-alumina catalyst to alumina. *Journal of Catalysis*, **33** (1), 145-148.
- Gardner, D. C., Bartholomew, C. H. (1981). Kinetics of carbon deposition during methanation of carbon monoxide. *Industrial Engineering Chemistry Product Research and Development*, **20** (1), 80-87.
- Ho, S. V., Harriott, P. (1980). The kinetics of methanation on nickel catalysts. *Journal of Catalysis*, **64** (2), 272-283.

- Huang, C. P., Richardson, J. T. (1978). Alkali promotion of nickel catalysts for carbon monoxide methanation. *Journal of Catalysis*, **51** (1), 1-8.
- Kester, K. B., Falconer, J. L. (1984). CO methanation on low-weight loading NiAl₂O₃: Multiple reaction sites. *Journal of Catalysis*, **89** (2), 380-391.
- Khodakov, A. Y., Chu, W., Fongarland, P. (2007). Advances in the development of novel cobalt Fischer-Tropsch catalysts for synthesis of long-chain hydrocarbons and clean fuels. *Chemical Reviews*, **107** (5), 1692-1744.
- Kikuchi, E., Morita, Y. (1969). Hydrogenolysis of n-pentane on nickel catalyst. *Journal of Catalysis*, **15** (3), 217-223.
- Klose, J., Baerns, M. (1984). Kinetics of the methanation of carbon monoxide on an alumina-supported nickel catalyst. *Journal of Catalysis*, **85** (1), 105-116.
- Kopyscinski, J., Schildhauer, T. J., Biollaz, S. (2010). Production of synthetic natural gas (SNG) from coal and dry biomass—A technology review from 1950 to 2009. *Fuel*, **89** (8), 1763-1783.
- Kramer, R., Andre, M. (1979). Adsorption of atomic hydrogen on alumina by hydrogen spillover. *Journal of Catalysis*, **58** (2), 287-295.
- Lim, J.Y., McGregor, J., Sederman, A.J., York, A.P.E. and Dennis, J.S. (2015). Kinetic studies of CO₂ methanation using a batch reactor over a Ni/ γ -Al₂O₃ catalyst. Paper accepted by *Chemical Engineering Science*. Doi: 10.1016/j.ces.2015.10.026.
- Lim, J.Y., McGregor, J., Sederman, A.J., York, A.P.E. and Dennis, J.S. (2016). Investigations of the Boudouard and the Water-gas Shift Reaction over a Ni/ γ -Al₂O₃ catalyst using a batch reactor. Paper in preparation, copy available from authors on request.
- Lyngfelt, A., Leckner, B., Mattisson, T. (2001). A fluidized-bed combustion process with inherent CO₂ separation; application of chemical-looping combustion. *Chemical Engineering Science*, **56** (10), 3101-3113.
- McGregor, J., Canning, A. S., Mitchell, S., Jackson, S. D., Gladden, L. F. (2010). The influence of carbon laydown on selectivity in the hydrogenation of pentenenitriles over supported-nickel catalysts. *Applied Catalysis A: General*, **384** (1), 192-200.
- Rochelle, G. T. (2009). Amine scrubbing for CO₂ capture. *Science*, **325** (5948), 1652-1654.
- Sanchez-Escribano, V., Vargas, L., Finocchio, E., Busca, G. (2007). On the mechanisms and the selectivity determining steps in syngas conversion over supported metal catalysts: An IR study. *Applied Catalysis A: General*, **316** (1), 68-74.
- Tøttrup, P. B. (1976). Kinetics of decomposition of carbon monoxide on a supported nickel catalyst. *Journal of Catalysis*, **42** (1), 29-36.
- Tada and Kikuchi, *Catal. Sci. Technol.*, **5**, 2061 (2015).
- Van Herwijnen, T., Van Doesburg, H., & De Jong, W. A. (1973). Kinetics of the methanation of CO and CO₂ on a nickel catalyst. *Journal of Catalysis*, **28** (3), 391-402.

Vance, C. K., Bartholomew, C. H. (1983). Hydrogenation of carbon dioxide on group VIII metals: III, Effects of support on activity/selectivity and adsorption properties of nickel. *Applied Catalysis*, **7** (2), 169-177.

Vannice, M. A. (1975). The catalytic synthesis of hydrocarbons from H₂CO mixtures over the group VIII metals: II. The kinetics of the methanation reaction over supported metals. *Journal of Catalysis*, **37** (3), 462-473.

Weatherbee, G. D., Bartholomew, C. H. (1982). Hydrogenation of CO₂ on group VIII metals: II. Kinetics and mechanism of CO₂ hydrogenation on nickel. *Journal of Catalysis*, **77** (2), 460-472.

Xu, J. & Froment, G.F. (1989). Methane steam reforming, methanation and water-gas shift: 1. intrinsic kinetics. *AI.Ch.E.J.*, **35**, 88-96.

Young, J. B., Todd, B. (2005) Modelling of multi-component gas flows in capillaries and porous solids. *International Journal of Heat and Mass Transfer*, **48** (25-26), 5338-5353.

Zhang, J., Fatah, N., Capela, S., Kara, Y., Guerrini, O., Khodakov, A. Y. (2013). Kinetic investigation of carbon monoxide hydrogenation under realistic conditions of methanation of biomass derived syngas. *Fuel*, **111**, 845-854.

Highlights

- CO methanation investigated in a spinning-basket reactor operated in batch
- Rate and selectivity determined for 12 wt% Ni/ γ -Al₂O₃ catalyst, 443–473 K to 16 bar
- Marked increase in rate after depletion of CO
- Selectivity for CH₄ markedly lower than in CO₂ methanation
- DRIFTS showed carbonyl species on Ni clusters and formate groups on different Ni sites